N62 55824

NACA TN 3824

NATIONAL ADVISORY COMMITTEE FOR AERONAUTICS

TECHNICAL NOTE 3824

EFFECT OF AN INTERFACE ON TRANSIENT TEMPERATURE DISTRIBUTION IN COMPOSITE AIRCRAFT JOINTS

By Martin E. Barzelay and George F. Holloway

Syracuse University



Washington

April 1957

NATIONAL ADVISORY COMMITTEE FOR AERONAUTICS

TECHNICAL NOTE 3824

EFFECT OF AN INTERFACE ON TRANSIENT TEMPERATURE DISTRIBUTION IN COMPOSITE AIRCRAFT JOINTS

By Martin E. Barzelay and George F. Holloway

SUMMARY

Geometrically related structural joints representing typical skin-stringer cross sections were tested under radiant heating to simulate the effects of aerodynamic heating. Temperature histories for 15 2024-T aluminum-alloy fabricated specimens and an equal number of integral control specimens were recorded for two different constant heat inputs, ranging from approximately 5 to 40 Btu/(sq ft)(sec). A maximum temperature rise of 450° F was attained in the specimens in 8 to 40 seconds of heating. There was no restraint or external loading applied.

The presence of an interface was found to have a significant effect on the temperature distribution in all geometries tested and thus must be considered in temperature calculations.

Interface conductance values were computed for each of the 15 fabricated specimens. These values ranged from approximately 150 to 1,300 Btu/(sq ft)(hr)(°F) with a modal value of 300 Btu/(sq ft)(hr)(°F). Geometry and heating rate were found to have an effect on joint conductance by influencing the temperature distribution and thus the warping of the mating surfaces.

INTRODUCTION

In the design of aircraft structures where aerodynamic heating is encountered, a knowledge of the temperature distribution within the structure is of considerable importance. While the problem can be solved by analytical, numerical, and analog methods in many cases, physical data upon which such analyses have to be based are still largely unavailable, especially those concerning the conductance (or its reciprocal, the contact resistance) across structural joints.

Although some knowledge of thermal contact conductance for aircraft joints is available from the work of references 1, 2, and 3 and from the work of other investigators in related fields discussed in reference 1,

the experimental data are far from complete. What is needed by the aircraft designer is a comprehensive body of data for contact conductance in terms of all pertinent variables, which will enable him to select a value or values to be used in calculations, whether analytical or numerical. The designer must also have a knowledge of the significance of interface conductance as it affects temperature distributions. The present program involving 2024-T fabricated skin-stringer combinations and including control specimens of integral construction examines this problem and provides new interface conductance data.

This investigation at Syracuse University was sponsored by and conducted with the financial assistance of the National Advisory Committee for Aeronautics. The contribution of Dr. Yi-Yuan Yu to the development of the more exact method of incorporating interface conductance in the numerical analysis of transient heat flow as explained in appendix B was appreciated.

SYMBOLS

A_f	flange cross-sectional area, sq in.
A_w	web cross-sectional area, sq in.
Ai, Bi	elements of infinitesimal thickness at interface
c	specific heat, Btu/(lb)($^\circ$F)
h	interface conductance, Btu/(sq ft)(sec)($^\circ$F) or Btu/(sq ft)(hr)($^\circ$F)
k	thermal conductivity, Btu/(in.)(sec)($^\circ$F)
l	length, in.
l_f	length of flange, in.
l_w	length of web, in.
q, Q, ΔQ	heat flow, Btu/(sq in.)(sec); also Btu/(sq ft)(sec)
t	time, sec
Δt	time interval, sec
t_f	thickness of flange, in.
t_s	thickness of skin, in.

t_w thickness of web, in.

T temperature, $^{\circ}F$ (referred, in general, to a zero reference); also $^{\circ}R$

T_f average temperature of flange, $^{\circ}F$

T_w average temperature of web, $^{\circ}F$

ΔT temperature drop across interface, $^{\circ}F$; also $T_{Ai} - T_{Bi}$

V volume, cu in.

ΔV elemental volume, cu in.

w specific weight, lb/cu in.

x, y, z space coordinates (fig. 4)

α nondimensional time parameter, $\frac{k}{c w \tau^2} t$

β constant in equations (B1) and (B2), $\frac{k \Delta t}{c w \tau^2}$

γ constant in equations (B1) and (B2), $\frac{q \Delta t}{c w \tau}$

δ thickness of equivalent air gap, in.

ϵ constant in equations (B2), $\frac{\Delta t}{c w \left(\frac{\tau^2}{k} + \frac{\tau}{h} \right)}$

τ thickness of skin, in.

φ nondimensional temperature parameter, $\frac{k}{q \tau} T$

Subscript:

i interface element in numerical analysis

DESCRIPTION OF APPARATUS

A general view of the test installation is shown in figure 1 and a detailed exploded view, in figure 2.

The apparatus may be divided into the following main groups:

(1) Bank of heating elements to supply radiant heat to the specimen. It consisted of uniformly spaced parallel graphite rods with a radiating area of 12 by 10 inches. Input terminals and series connectors were mounted on Marinite insulator plates. The maximum current drawn from the three-phase, 110-volt supply was 370 amperes, corresponding to a 125-kilowatt power dissipation. A maximum surface temperature of 3,800° F was reached by the graphite rods about 10 seconds after the power was connected. Because of rapid oxidation and gassing the useful life of the graphite elements was about $2\frac{1}{2}$ minutes.

A reflector, made of 3/8-inch-thick 6061-W polished aluminum-alloy plate, helped to minimize losses.

(2) Movable curtain to intercept radiation during the warmup period and then to provide a step input of such radiation. It consisted of a 1-inch-thick plate of Marinite faced with a thin layer of poured-in-place Blazecrete.

(3) Adjustable frame to mount specimen.

(4) Temperature recording instrumentation. The output of the thermocouples was read directly on a Century, Model 408, multichannel recording oscillograph. All galvanometers had a nominal sensitivity of 12 microamperes per inch of deflection on the recording paper.

The thermocouple leads from the specimen were connected to the oscillograph through a specially built calibrator, the circuit diagram of which is given in figure 3. The function of the calibrator was to take into account the total resistance of each matched thermocouple-galvanometer loop and to adjust the galvanometer sensitivity, with the aid of a variable-series resistor, so that a given voltage signal from the thermocouple (i.e., a given temperature) corresponds to any desired trace deflection. All channels could be calibrated in a minimum time before each test.

(5) An electric timer was inserted parallel to the main power circuit to measure the total heating period of a cycle and the life of the heating elements accurately. In addition, the motion of the curtain actuated a limit microswitch which energized an auxiliary galvanometer in the oscillograph. The resulting signal defined the time limits of the step heat input in relation to the transient temperature traces.

TEST PROCEDURE

Theoretical Basis and Testing Technique

The aerodynamic heating of the outside skin surface of a high-speed aircraft depends on a multiplicity of factors not pertinent to this investigation. To facilitate an experimental approach, the aerodynamic heating may be replaced by radiant heating if the latter can be adjusted to simulate approximately the boundary conditions encountered in actual high-speed flight. This is so because for given boundary conditions the temperature distribution and heat-flow pattern within the structure are unique regardless of the source of heat energy. In many cases the complexity of a flight mission and the resulting aerodynamic heating schedule cannot be conveniently duplicated by a radiant heating apparatus of limited control. It is clear, however, that a simple heat input, such as one which is constant with time and uniformly distributed over the surface, gives as much insight into the effect of interface conductance on the temperature distribution as would be afforded by an arbitrary choice from the large number of possible boundary conditions.

In actual testing, therefore, unidirectional radiant heating of short duration has been utilized. For this case those faces of the structure which are not subjected to heating can be regarded as insulated. The heat input was assumed uniform in the central area of the specimen where measurements are made. Thus, since the cross section is uniform at any plane perpendicular to the z-axis (fig. 4) the heat flow can be considered two-dimensional.

The specimens were at a uniform room temperature at the beginning of each test and only the temperature rise was recorded.

To check whether the assumption of uniform heating was valid and to establish the boundaries of the working area, flat plates were heated under the same conditions as were the test specimens. Because of the size of the heated area (10 by 10 inches) in relation to the distance which had to be maintained between the heater bank and specimens, the end effects were quite pronounced. The temperature distribution over the entire area of the flat plate was approximately hyperbolic in both the x- and the z-directions, with the point of highest temperature located at the geometrical center. The isotherms were approximately elliptical in shape. On the basis of these isotherms it was thought advisable to concentrate all measurements in a central 4- by 4-inch area where the variation of temperature was found to be within a limit of ± 2 percent. The central region will, of course, lose heat by conduction to the cooler outer regions, but the relative amount of this heat loss is negligible in its influence on the temperature distribution over the central area.

The validity of assuming a constant rate of heat input to the specimen must also be considered. The previously discussed tests with flat plates indicated that, except in the initial heating period of up to 2 seconds, the heat input from the radiant-heating source is virtually constant for the period of testing. The addition of a stringer to the flat plate causes local lowering of the plate temperature; but, if the temperature of the radiant heater is always far in excess of that of the absorbing body, that is, if $T_1 \gg T_2$, then as a consequence of the Stefan-Boltzmann fourth-power law the effect of local variation in T_2 may be neglected. Some slight deviation in heat flow may also be expected as source temperature, emissivity, and plate absorptivity change, but these effects may be neglected for comparative tests of fabricated and integral specimens.

In order to achieve several different heat inputs to the specimen, a suitable coating was applied to the receiving surface to change its radiation absorptivity.

With the foregoing boundary conditions over the area under scrutiny, the tests provided temperatures at chosen points along the heat-flow path during the transient heating cycle. On the basis of these representative temperature functions $T(x,y,t)$, heat-flux lines and isotherms could be established.

The measurement of radiant heat input in the transient case was accomplished by calculating the increase of total heat content of the elemental volume in the irradiated surface of the specimen with the highest value of $\partial T/\partial t$. For such an elemental volume, located some distance away from the bulk of the stringer, only a negligible part of the heat received by radiation is conducted away; therefore, most of the heat is used to raise the temperature. Accordingly, the average heat input into such an elemental volume can be approximated by

$$\Delta Q = \Delta V c w \frac{\partial T}{\partial t} \tag{1}$$

The quantity $\partial T/\partial t$ is available from the records for the particular surface element. This heat input is then taken as being a constant for the whole skin area near the stringer where the measurements are concentrated. A sample calculation of heat input is carried out in appendix A. This method of computing actual radiant heat input at the boundary plane was found to be superior to indirect calculations based either on the constants of radiation or on the electrical energy delivered to the heater.

The same principle of inferring heat-content rise from temperature rise was helpful in computing the conductance of the interface. First,

the primary data yielded an average interface temperature drop ΔT as a function of time. The other quantity necessary to determine the conductance, the heat passing through a unit area of the interface per unit time, was computed to a good degree of approximation from the rate of increase of heat content of the entire structural mass downstream from the interface. A sample calculation of the interface conductance is also presented in appendix A.

Description of Specimens

The test specimens consisted of the aluminum-alloy skin-stringer combinations shown in figure 4. Dimensions are tabulated in table I. Although these specimens were typical of aircraft construction insofar as possible, dimensions were chosen to give a wide range of dimensional ratios.

In the fabricated group of specimens the flange of the extruded T-section was attached to the skin by two rows of standard countersunk rivets. The rivet pitch was kept at a uniform $1\frac{1}{2}$ inches. Rivets were type AD-2, AD-3, and AD-4 (see table I).

Each fabricated specimen had its integral dimensional counterpart, but the integral specimens were machined from solid 2024 stock and thus lacked the interface joint. The integral specimen in each case served to compare the temperature distribution in an uninterrupted heat path with that of a riveted structural joint. In order to utilize available extrusions and because of difficulties in machining, each control specimen was made up of two identical halves joined along the center plane of the web by one or two rows of small rivets. This was possible because the plane passing through the center of the web is a plane of symmetry, as shown in figure 4. Since all isotherms crossing this plane are necessarily normal to it at the point of intersection, no net heat flow will take place through it.

The control specimens were machined from annealed 2024-O extrusions to avoid stress relief and resulting warping during fabrication. The material of the riveted specimens was 2024, both clad and unclad, with various manufacturing heat treatments (-O, -T3, -T4, and -T6). These heat treatments correspond to different thermal conductivities. In addition, the conductivity varies over the temperature range of the tests. The latter effect is partly due to unavoidable metallurgical transformations that take place in the aluminum alloy during the heating cycle. The combined effect of all these possible changes on temperature distribution is examined in the section "Precision of Data." For the purposes of calculation, it was assumed that the value of thermal conductivity for all specimens remained constant at 0.002 Btu/(in.)(sec)($^{\circ}$F).

Because of time limitations, only one cross-sectional location in each specimen was investigated. This location was chosen to be 3/4 inch (half of rivet pitch) from the center line of the specimen along the stringer for both the riveted and integral specimens.

Thermocouple Technique

The preparation of thermocouples followed the practice recommended in reference 4. Factory-calibrated iron-constantan No. 30 gage thermocouple wire with braided Fiberglas insulation was used throughout the tests. This was the smallest practical size, considering the required accuracy of temperature measurements as well as the ease of fabrication and handling. The bead was formed by a high-intensity spark from a graphite electrode.

Thermocouple locations and a typical installation are shown in figure 5. Since some of the holes would overlap in the same cross section, as shown in figure 5, it was necessary to offset them slightly along the length of the stringer. This offset, which never exceeded 3/8 inch, is permissible since the heat flow is essentially two-dimensional in the test area.

In making thermocouples, after the bead was formed a length of the outside insulation was stripped. This part of the leads, which was to lie inside the hole, was then dipped in Glyptal lacquer to prevent fraying and to provide electrical insulation.

The thermocouples were cemented into the holes with a copper-base dental cement, a quick-setting material with good heat-conduction properties. Those thermocouple beads which were installed in shallow holes 1/16 inch or less in depth had to be peened around the mouth of the hole to obtain firm anchoring, as shown in figure 5. Care was taken to assure bottoming of the thermocouple beads and additional anchoring was provided by a small amount of Sauereisen No. 1 cement.

Conduct of Tests

The specimen was mounted by the four corners in the supporting frame, shown in figure 1, in such a manner that free expansion and bending were possible. The outside skin faced the bank of heating elements at a uniform distance of 3 inches.

The test sequence was as follows:

(1) Calibrate thermocouples and galvanometers

(2) Activate oscillograph

(3) Energize heating elements

(4) Allow heating elements to reach a maximum temperature (time required was approximately 8 seconds)

(5) Raise curtain to give step heat input

(6) Visually follow temperature traces on the oscillograph screen until the maximum rise reaches a point corresponding to 450° F above room temperature

(7) Lower curtain to end step heat input

(8) Cut off power to the heater

In general, all specimens were tested with two different heat flows, ranging from approximately 5 to 40 Btu/(sq ft)(sec). A low heat flow was achieved by leaving the specimen surface bare, thus utilizing the relatively low absorptivity of polished aluminum. The average heat input under these conditions was 8 Btu/(sq ft)(sec). A high heat flow of approximately 29 Btu/(sq ft)(sec) was attained by coating the irradiated face with Superflake graphite coating.

Depending on heat input, the duration of the tests varied from 8 to 40 seconds.

PRECISION OF DATA

The sources of error could be divided into the following main groups:

(1) Failure to attain the prescribed boundary conditions.

It was mentioned in the section "Theoretical Basis and Testing Technique" that the uniformity of heating over the exposed area of the specimen deviated from the ideal and, furthermore, that a constant time rate of heating was not completely attainable because of limitations inherent in the radiant-heating setup.

The nonuniformity of heat input was aggravated by the variation of local absorptivity on the specimen as verified by local temperature readings in the skin. This nonuniformity may be attributed to minor variations in bare surface finish or in thickness of the graphite coating.

Another phenomenon contributed to the nonuniformity of heat flow. The commercial-grade graphite heating elements did not have uniform qualities so that hot spots and cooler areas occasionally developed in

the heater bank. Even though the separation between the heater and specimen was relatively large, these local effects were noticeable in the results.

The assumption of the perfect insulation over the unheated surfaces was, of course, only approximated; these surfaces were being cooled by convection and radiation at a rate proportional to the temperatures attained.

The above-mentioned deviations from idealized boundary conditions are of relatively the same magnitude for all tests and therefore do not significantly influence the comparisons which are made between specimens. However, when comparison is to be made between experimental and analytical results, it is more convenient to base the calculations on simplified boundary conditions than to include all the variables inadvertently introduced in the experiments. It is for this reason that efforts were made to approximate uniform and constant heat flow as closely as possible.

(2) Variation in original conductivity and changes taking place during the heating cycle.

Since the specimens used in the test program varied in original heat treatment, there was a substantial difference in thermal conductivity from specimen to specimen. It is also known that conductivity is a function of the temperature level. Unfortunately, the effect of temperature level cannot be isolated because the various heating cycles cause metallurgical phase transformations which can result in larger fluctuations in the conductivity value of the aluminum alloy than do differences due to original heat treatments. The seriousness of the problem is seen in reference 5, where, in the temperature range of 200° to 700° F, the conductivity value of the 2024 alloy is reported to vary as much as ±13 percent from the mean without any clear tendency as to the direction. Consequently, in comparing experimental temperature distributions in the present test program, the conductivity variations represent an uncontrollable variable.

Obviously, the choice of a constant average thermal-conductivity value of 0.002 Btu/(in.)(sec)(°F) for the calculations involves some error when a comparison between experimental and analytical temperature distributions is made. The particular heating history of the specimen probably corresponds to a very complicated local phase-transformation pattern which cannot be traced and incorporated in the analytical treatment of the problem. The assumption of a constant thermal conductivity is thus dictated by necessity. It is expected, however, that for any aerodynamic-heating schedule based on actual flight conditions the value will remain within the percentage variation found in reference 5.

(3) Errors in local temperature measurements due to imperfections in lead wire and thermocouple bead, installation, and response lag.

The thermocouple wire was of high quality with calibration guaranteed by the manufacturer. Calibration of individual thermocouple assemblies was not considered necessary. The thermocouple bead was formed by a standardized and uniform process and the soundness of fusion was inspected under magnification. Care was taken to insure proper insulation of the leads for their entire length, but some small leakage between the two leads may have been possible.

A uniformly good heat-conduction path between the sensitive element and the surrounding material was not completely attainable. The couples placed in shallow holes were especially sensitive in this respect and offered the greatest chance for a poor thermal contact. The shallow installations were also the most susceptible to loosening of the thermocouples during handling after repeated heating cycles had made the cements brittle.

The thermocouple response lag was considered negligible because of the small mass of the bead. Furthermore, for the comparative results sought, all such lags would be of the same order of magnitude.

Based on experience, the conclusion can be drawn that the effects of the above-mentioned possible sources of error are of minor consequence and certainly of less effect on the data than those of items (1) and (2) above.

(4) Assumption of linearity of scale factors.

In calculating temperatures from galvanometer readings it was assumed that the output of the iron-constantan thermocouples was linear from 0° to 500° F. This assumption introduced an error not exceeding ± 2 percent in the temperature readings but greatly simplified the evaluation of the large volume of data taken. The linearity of the galvanometer deflection was found to be satisfactory, thus affording a linear interpolation between zero and a single calibration point in the upper temperature ranges.

As a consequence of the above assumptions, it was possible to use a single scale factor in converting oscillograph-trace deflections into temperature rise. The total errors thus introduced probably remained within ± 3 percent.

In discussing the precision of data it must be realized that extreme precision was unattainable but was unnecessary. The large number of temperatures measured in each test and the symmetry of thermocouple locations made it evident that material and manufacturing variables have a large and

often unpredictable influence on temperature distribution in the types of joints tested. The accuracy of temperature measurements, therefore, cannot be stated in terms of probable percentage deviation with any hope of great reliability. A value of ±6 percent may be estimated, however, on the basis of experience.

What is of utmost importance, however, is the conclusion that the comparative differences in temperature distributions found in the present tests are of such substantial magnitude that a cumulative total error of ±6 percent in temperature measurement does not affect the conclusions of this report; that is, there is no danger that errors of this magnitude affect one comparative item and not the other.

The values of interface conductance presented herein are estimated to be correct within ±15 percent.

RESULTS

A minimum of two tests, corresponding to two different heat inputs, was run with each specimen.

The data for each test consisted of temperature-time records for 16 selected locations in the specimen. Whenever the instantaneous temperature gradients appeared to be small, that is, well within the expected error in temperature measurement, a group of readings was reduced to a single value by averaging. This was possible, for instance, in the flange of the stringer where the temperature gradients were often negligibly small. The 16 traces could thus be reduced to 5 to 8 representative temperature-time records. Curves of this type are given for one pair of specimens (integral and riveted) in figure 6. It was considered unnecessary to present the complete temperature records.

An examination of the two records of figure 6 readily discloses the disturbance caused by the introduction of an interface. The points in the web and flange downstream from the interface are especially affected; the points in the skin under the flange are influenced to a small degree.

All points appear to approach a constant rate of temperature rise as the heating is continued at a uniform rate. The trend observed may be predicted by theoretical analysis of the problem; the temperature differences across the section become stabilized and all temperatures then rise at a constant rate. Thus, the temperature difference at the interface of a riveted specimen ΔT also approaches a limit.

In figure 7(a) are shown the results of two tests run with two different heat inputs (10.8 and 18.6 Btu/(sq ft)(sec), respectively). When

these data are replotted on a nondimensional basis as in figure 7(b), the two sets of curves nearly coincide. The pair of tests, the results of which are presented in figures 7(a) and 7(b), was run with an integral specimen; riveted specimens heated at different rates revealed the same tendency with a slightly poorer coincidence between the two tests.

In the course of determining the effect of interface on temperature distribution in joints of different geometry, interface conductance values were determined for each of the 15 fabricated specimens. A tabulation of these conductance values, showing the minimum and maximum obtained in each test, is given in table II. The computed equivalent air-gap thickness for each specimen is also given in this table. In addition, the approximate conductance-time history of each specimen is plotted in figures 8(a), 8(b), and 8(c). The two different test series indicate two different heat flow rates. (See also table II.)

An examination of the conductance values leads to the following observations:

(1) Interface conductance varied over a considerable range in the 15 fabricated specimens. Attempts to relate geometrical variables, rivet size, and interface conductance, however, were unsuccessful, probably because of the fact that the limited number of specimens in the program did not allow a thorough examination of the effect of any single geometrical or riveting variable on interface conductance. Furthermore, no given group of specimens, prepared in one shop, displayed any special characteristics when compared with a group fabricated in a different shop, presumably under somewhat different manufacturing practices and tolerances.

(2) For a given interface conductance the transient temperature drop across the interface depends on the mass of the stringer and its geometrical distribution with respect to the size of the contact surface. It was found that the larger the bulk of the stringer downstream of the interface, the longer it took for this bulk to reach a given temperature. As a consequence of the larger time delay in the heating of a bulky stringer, larger instantaneous temperature differences developed between the skin and the stringer.

(3) During one given test of short duration the conductance value varied as much as ± 25 percent with no clear trend either with time or with increasing mean interface temperature.

(4) Upon repeating a test on the same specimen, regardless of whether low or high heat input was applied first, a lower conductance value was found in 13 out of 15 cases. With the first runs averaging an interface conductance value of 525 and the second runs, a value of 401 Btu/(sq ft)(hr)($^{\circ}$F), the average drop between the two runs was

23.6 percent. If the contact resistance is expressed in terms of an equivalent air-gap thickness based on air thermal conductivity at 75° F, the value 525 Btu/(sq ft)(hr)(°F) corresponds to 0.00034 inch and the value 401 Btu/(sq ft)(hr)(°F), to 0.00045 inch.

(5) The extreme values of conductance found in the entire course of the investigation were 156 and 1,310 Btu/(sq ft)(hr)(°F) corresponding to an air-gap thickness of 0.00115 and 0.00014 inch, respectively.

It should be pointed out here that the dimensions of the two different specimens (specimens 4 and 5) showing these extreme conductance values were very similar. On the other hand, specimens of entirely different configuration (e.g., specimens 7 and 14) revealed a remarkable agreement in the interface conductance value.

(6) The overall average of conductance found for the 15 riveted specimens was 463 Btu/(sq ft)(hr)(°F), while the overall average air gap was 0.00039 inch.

DISCUSSION

As explained in the "Introduction," the chief purpose of the present investigation was to assess the importance of the interface conduction as a factor to be considered in determining temperature distributions in aircraft structures. An examination of the data presented in the section "Results" shows that interface conductance must be taken into account for any geometry. This is explained further in the following paragraphs.

Geometry and Temperature Distribution

In figure 6 typical transient temperature distributions of the type available for all specimens in the program were presented for a single fabricated specimen and for its integral control. The effect of the interface on the temperature distribution may be seen in comparing the two sets of curves. It is apparent that for the geometrical configuration shown any temperature distribution found by a calculation which neglected the interface discontinuity would be seriously in error.

In figures 9(a) and 9(b) the experimental temperature histories of two selected points in each of two different geometries (specimens 8 and 3) are presented to show the relative importance of the interface. It can be seen that temperature histories of points such as A and B (fig. 9) are influenced by an interface to a widely different extent in the extreme cases of specimens 8 and 3; there is a very slight disturbance in specimen 8 (in comparison with control specimen 8C) but a

large disturbance in specimen 3 (in comparison with control specimen 3C) due to addition of the interface. This distinctly different influence of an interface (with the same average conductance) indicates how temperatures at corresponding points can be affected in different joint configurations.

The temperature history of selected extreme points in a cross section, however, cannot be a basis for the stress analysis which obviously must be based on temperature distribution over the entire structure. Thus, geometry, interface conductance, and rate of heating must all be taken into account and it would not be warranted to make general, simplifying assumptions to establish the limits of critical conditions in terms of any of the above variables. In other words, until the precise use of interface conductance in a particular design problem is known, its final importance on structural behavior cannot be assessed; hence, its value should be included in any temperature-distribution calculation.

Some examples of the effects of an independently varying interface conductance on upstream and downstream temperature histories are shown in figures 10(a) and 10(b). Temperature histories were calculated for several arbitrary interface conductances by the method outlined in appendix B. In figure 10(a) the results of a trial set of calculations are shown with the conductance varying from 200 Btu/(sq ft)(hr)($^{\circ}$F) to infinity, that is, to the case of the integral specimen. In figure 10(b) the calculation is continued for the conductance value which seemed to fit the experimental data best. Minor differences between the calculated and experimental curves can be attributed to the deviation from constant heat input assumed in the calculation. What is important in these figures is that the correspondence of the calculation with the experimental data is dependent on the correct choice of interface conductance. It is obvious that a wrong choice of interface conductance for use in calculations can lead to a serious error in temperature distribution.

In figure 11 the transient temperature drop across the interface is plotted against skin temperature (at the stringer) for all geometries tested. Selections have been made from figure 11 and replotted in figures 12(a) to 12(d) for various groupings of geometrical variables. It is clear that the mass of the stringer and its geometrical distribution with respect to the size of the contact surface have a marked effect on the interface temperature drop. It can be stated as a general rule on the basis of figure 11 that the larger the bulk of the stringer downstream of the interface, the larger the transient temperature drop becomes for a given set of conditions. The curves of figure 11 are affected by the random value of the joint conductance; therefore, the geometrical variables cannot be independently evaluated from this viewpoint. While calculations show that the effect of conductance is not sufficient to displace the qualitative positions of the curves with respect to one another, precise relationships could be established only if the interface conductance value were a fixed quantity in all cases.

Evidence gathered in the course of this investigation indicates that the thermal conductance of practical joints is not independent of geometry. Joint conductance is defined here as some average value of local conductances over the interface and is computed from experimental data by the method outlined in appendix A.

It is assumed that all joints manufactured under the same conditions have nearly the same initial contact and conductance value (before heating). However, as soon as distortion of the mating parts occurs because of unequal heating, this phenomenon may also involve a change in the intimacy of contact and result in interface conductance variation (this reasoning will be further elaborated on in the section "Heating Rate and Temperature Gradients"). Since temperature distribution and warping are both functions of geometry, it is probable that geometry controls the value of interface conductance during the time of heat flow, although insufficient data were available to reveal a consistent relationship.

Heating Rate and Temperature Gradients

Because of the transient heating conditions and the variable cross section of the heat path (in the xy plane) the temperature gradients are nonuniform in a heated skin-stringer joint. The largest of these gradients in a continuous configuration is encountered at the directly heated surface immediately after the start, if the input is uniform. When the joint contains an interface discontinuity, the temperature across the interface will also be discontinuous and there will be a very high gradient at this location.

It seems evident that, even though the joints tested were unrestrained, the nonuniformity of temperatures and temperature gradients must cause internal stresses in the structure whether it is integral or riveted. It is not within the scope of present work to analyze thermal stresses and find relations between temperature distributions, deformations, and the resulting changes of interface contact in a riveted specimen. Nevertheless, it is easy to see that the changes in temperature distribution from one specimen configuration to another and especially from the integral to riveted version of the same configuration must be reflected in changes of stress distribution and deformations.

It was also observed in the experiments that interface conductance varied from test to test in the same specimen and even during one heating cycle. The variation in the intimacy of contact is believed to be related to changes in the temperature distribution pattern. This pattern, of course, changes constantly during transient heating whether the heating is uniform or nonuniform. Warping and the related changes in interface conductance can thus be regarded as functions of heating time.

Experimental evidence indicates that temperature distribution and contact conductance may be mutually interdependent. However, because of the uncertain nature of the warping the interface conductance value could not be conveniently related to temperature distributions (or heating rates) in the present work. It is sufficient to point out that the heating rates employed in this testing program and the temperature distributions thus attained were responsible for certain physical changes at the interface which resulted in a ±25-percent random fluctuation in interface conductance value.

Interface Conductance

In references 1 and 2 the factors influencing the thermal conductance of interfaces were studied and values were obtained for this conductance. It was found that the value of interface conductance is a function of the conductivity, hardness, strength, warping, and oxidation properties of the two joint-forming bodies. Furthermore, the conductance was found to depend on the mean temperature level, the pressure exerted on the interface area, the surface roughness and flatness, the condition of gases and impurities entrapped between the joined surfaces, and the loading and heating history of the joint.

In these past investigations the test specimens and conditions were chosen to yield a maximum of information about interface conductance. In the series of tests reported herein the specimens were more nearly representative of practical aircraft construction and were tested under transient heating conditions. The values of interface conductance obtained in the course of these tests are given in table II and plotted in figures 8(a) to 8(c), as noted under "Results."

Because of the small size of the interface area in each case and the limitations in the instrumentation it would have been very difficult, and also impractical, to determine the distribution of interface conductance along the line of joint contact in a cross section, so that a single average value was computed as noted above under "Geometry and Temperature Distribution."

The possible effects of geometry and heating rates on interface conductance were discussed above.

While interface conductance was found, in general, to increase with mean interface temperature level in references 1 and 2, no such consistent trend was noticeable in the present tests since the warping precluded the isolation of the mean interface temperature as an independent variable.

The effect of rivet size, material, and spacing was not studied. There is some evidence based on yet unpublished data obtained by the

authors to the effect that the joint conductance increases with the size of the rivets. In addition, there is a positive indication that local conductance varies noticeably with distance from rivets even when the rivet pitch is kept low.

Warping of the skin and stringer could be visually observed during each test. In some specimens a visible air gap opened at some contact points after the initial heating. It is believed that rivet yielding and slippage at critical locations took place at elevated temperatures.

It can be deduced from the above discussion that since contact conductance depends on a complex set of conditions some scatter in its value can be reasonably expected. It is thus not considered unusual that conductance values found in this investigation ranged approximately from 150 to 1,300 Btu/(sq ft)(hr)($^{\circ}$F). The arbitrarily large number of experimental conductance values was plotted on a standard distribution curve (not shown) which yielded a statistical mode of 300 Btu/(sq ft)(hr)($^{\circ}$F) for all tests.

It is of some interest to compare the interface conductance values obtained in this investigation with those measured in references 1 and 2.

In the tests of reference 1, 1-inch-thick 7075-T6 aluminum-alloy specimens of various surface roughnesses formed interfaces and the conductance of these interfaces was measured at temperatures up to 450° F in steady-state heat flow and at a constant contact pressure of 7 psi.

Despite the differences between the test conditions of reference 1 and those of the present investigation, the extremities of interface conductance value in reference 1 were nearly the same, 210 and 1,350 Btu/(sq ft)(hr)($^{\circ}$F), as in the present work. However, the value occurring with the greatest frequency in reference 1 was much higher than the mode in the present tests. This was obviously due to the special care taken with most specimens during the machining and assembling of the surfaces in the earlier tests, while in the present tests plates and extrusions of standard finish and flatness were used to represent average aircraft practice.

In reference 2 the interface conductance extremities were 280 and 2,050 Btu/(sq ft)(hr)($^{\circ}$F), respectively, at 5-psi contact pressure until the heating and loading history caused a shift in conductance, in general, to progressively higher values upon return to the 5-psi pressure. Permanent surface changes due to the combination of high temperatures and pressures were, of course, not expected to occur in the present tests where the average contact pressure always remained at a low value, estimated to be of the order of 10 psi.

CONCLUSIONS

The following conclusions were derived from an investigation of the effect of an interface on the transient temperature distribution in composite aircraft joints.

1. The temperature distribution pattern in a heated structural joint of given geometry changes markedly with the introduction of an interface. The extent of this change depends on the value of interface thermal conductance.

2. Numerical solutions reveal that the temperature distribution pattern is also sensitive to changes in the interface conductance value.

3. Although the disturbance caused by an interface may not influence temperatures appreciably at certain remote locations in the structure, the value of interface conductance must be included in calculations of complete temperature distributions for stress-analysis purposes.

4. The experimentally determined interface conductance may vary over a considerable range from specimen to specimen, from one test run to the other, and even during a given test of short duration. In the present program the range of values extended from approximately 150 to 1,300 Btu/(sq ft)(hr)($^{\circ}$F), while the most representative value in the 15 interface specimens was 300 Btu/(sq ft)(hr)($^{\circ}$F).

5. It is indicated that the thermal conductance of practical joints is not independent of geometry. Different configurations may have the same initial conductance value; however, unequal heating must cause distortions, resulting in a change of contact and conductance. Geometry may thus control indirectly the value of interface conductance during heating.

6. In a given interface joint any change in temperature distribution results in a different deformation pattern and thus may be responsible for interface conductance variation. Such changes take place constantly during transient heating. Different heat inputs also create different boundary conditions for temperature distribution. The contact conductance and temperature distribution, therefore, appear to be mutually interdependent.

Syracuse University,
Syracuse, N. Y., March 15, 1956.

APPENDIX A

SAMPLE CALCULATIONS

The calculation of the radiant heat input q for specimen 12 is as follows:

(a) From the oscillograph record the rate of temperature increase of a point in the skin 2 inches from the center line is

$$\frac{\partial T}{\partial t} = 13.5^{\circ} \text{ F/sec}$$

(b) The volume of the skin with 1 square inch of heated area is

$$V = 0.25 \text{ cu in.}$$

(c) The product of the specific heat c and the specific weight w is

$$cw = \left[0.22 \text{ Btu/(lb)}(^{\circ}\text{F})\right](0.10 \text{ lb/cu in.})$$

$$= 0.022 \text{ Btu/(cu in.)}(^{\circ}\text{F})$$

(d) The heat received by 1 square inch of the outer skin surface in 1 second is

$$q = (V)(cw)\frac{\partial T}{\partial t}$$

$$= (0.25)(0.022)(13.5)$$

$$= 0.07425 \text{ Btu/(sq in.)(sec)}$$

$$= 10.7 \text{ Btu/(sq ft)(sec)} \qquad \text{(A1)}$$

The calculation of the interface conductance h for specimen 11, 30 seconds after the start of the test, is as follows:

(a) From the oscillograph record the average rate of temperature increase, at 30 seconds, of the flange area is

$$\frac{\partial T_f}{\partial t} = 7.6^\circ \text{ F/sec}$$

The average rate of increase, at 30 seconds, of the web area is

$$\frac{\partial T_w}{\partial t} = 7.1^\circ \text{ F/sec}$$

The approximate average temperature difference at the interface, at 30 seconds, is

$$\Delta T = 50^\circ \text{ F}$$

(b) The flange area is

$$A_f = 0.1563 \text{ sq in.}$$

The web area is

$$A_w = 0.1563 \text{ sq in.}$$

The length of the flange in contact with the skin is

$$l_f = 1.250 \text{ in.}$$

(c) The transient heat flow across 1 square inch of the interface area per second, at 30 seconds after the start of the test, is

$$\begin{aligned} q &= \frac{cw}{l_f}\left(\frac{\partial T_f}{\partial t} A_f + \frac{\partial T_w}{\partial t}\right)A_w \\ &= \frac{0.022}{1.25}(7.6 \times 0.1563 + 7.1 \times 0.1563) \\ &= 0.04045 \text{ Btu/(sq in.)(sec)} \end{aligned} \qquad \text{(A2)}$$

(d) By definition,

$$h = q/\Delta T$$

$$= \frac{0.04045}{50}$$

$$= 8.09 \times 10^{-4} \text{ Btu/(sq in.)(sec)}(^{\circ}\text{F})$$

$$= 419 \text{ Btu/(sq ft)(hr)}(^{\circ}\text{F})$$

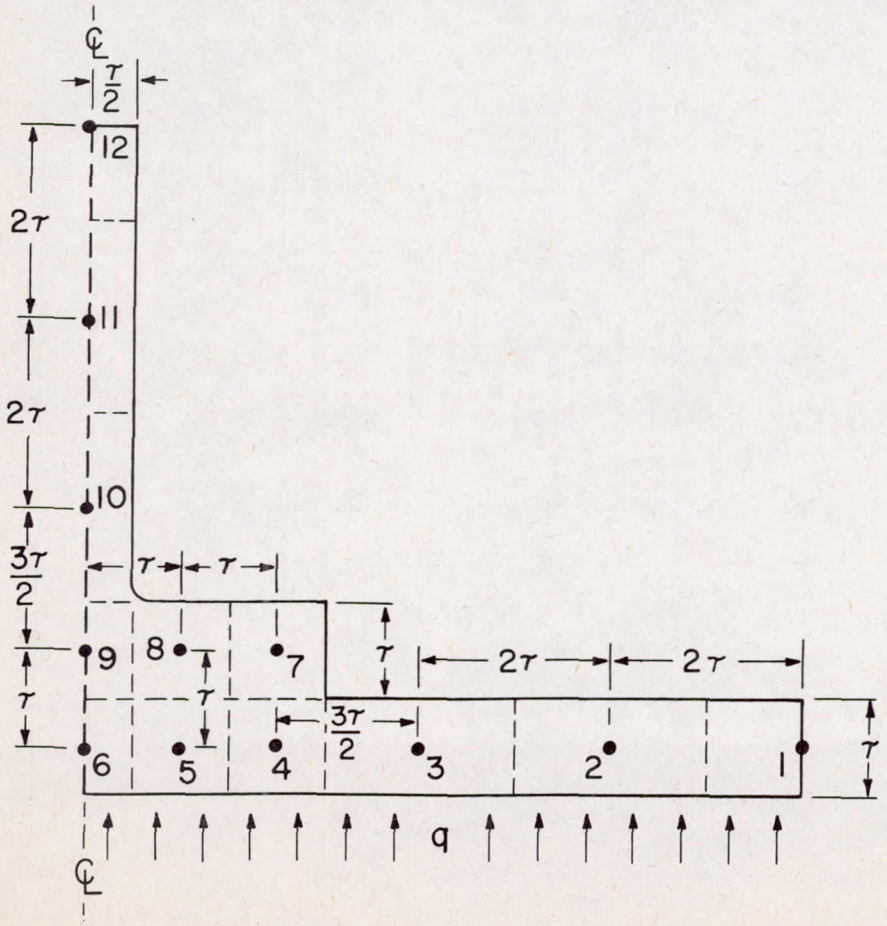
APPENDIX B

NUMERICAL SOLUTIONS

Numerical solutions of two-dimensional transient-heat-flow problems by lumped parameter methods have received considerable attention in recent years, as in references 6, 7, and 8. In reference 9 the details of a so-called marching process, where the temperature of each lump is found at the end of successive finite time intervals, is outlined. A similar solution is presented in reference 8 in a form adaptable to analog computation.

The method of reference 9 was used to carry out numerical calculations for the integral specimen. After modification to incorporate the effect of interface discontinuity, the method was similarly used for fabricated specimens. Two such modifications were introduced and are presented below, followed by a discussion of their relative merits. The general method of handling arbitrary geometry and boundary conditions follows:

The cross section of integral specimen 14C, divided at the plane of symmetry, can be lumped in the following manner: The smallest lumps are taken where the largest gradients are expected, as in the following sketch:



The next step is the writing of transient-heat-balance equations for each lump of unit thickness. For instance, the equation for unit thickness for lump 4 is

$$q\tau + \frac{k\tau}{3\tau/2}\left(T_3 - T_4\right) + \frac{k\tau}{\tau}\left(T_5 - T_4\right) + \frac{k\tau}{\tau}\left(T_7 - T_4\right) = c w \tau^2 \left(\frac{T_4' - T_4}{\Delta t}\right)$$

and, for lump 9,

$$\frac{k\tau/2}{\tau}\left(T_6 - T_9\right) + \frac{k\tau}{\tau}\left(T_8 - T_9\right) + \frac{k\tau/2}{3\tau/2}\left(T_{10} - T_9\right) = (c w \tau^2/2)\left(\frac{T_9' - T_9}{\Delta t}\right)$$

The 12 equations of the above type can now be simplified and expressed explicitly for the temperature of each lump at the end of each time interval, yielding the following expressions:

$$\left.\begin{aligned}
T_1' &= \gamma + \left(1 - \frac{\beta}{2}\right)T_1 + \left(\frac{\beta}{2}\right)T_2 \\
T_2' &= \gamma + \left(\frac{\beta}{4}\right)T_1 + \left(1 - \frac{\beta}{2}\right)T_2 + \left(\frac{\beta}{4}\right)T_3 \\
T_3' &= \gamma + \left(\frac{\beta}{4}\right)T_2 + \left(1 - \frac{7}{12}\beta\right)T_3 + \left(\frac{\beta}{3}\right)T_4 \\
T_4' &= \gamma + \left(\frac{2}{3}\beta\right)T_3 + \left(1 - \frac{8}{3}\beta\right)T_4 + (\beta)T_5 + (\beta)T_7 \\
T_5' &= \gamma + (\beta)T_4 + (1 - 3\beta)T_5 + (\beta)T_6 + (\beta)T_8 \\
T_6' &= \gamma + (2\beta)T_5 + (1 - 3\beta)T_6 + (\beta)T_9 \\
T_7' &= (\beta)T_4 + (1 - 2\beta)T_7 + (\beta)T_8 \\
T_8' &= (\beta)T_5 + (\beta)T_7 + (1 - 3\beta)T_8 + (\beta)T_9 \\
T_9' &= (\beta)T_6 + (2\beta)T_8 + \left(1 - \frac{11}{3}\beta\right)T_9 + \left(\frac{2}{3}\beta\right)T_{10} \\
T_{10}' &= \left(\frac{\beta}{3}\right)T_9 + \left(1 - \frac{7}{12}\beta\right)T_{10} + \left(\frac{\beta}{4}\right)T_{11} \\
T_{11}' &= \left(\frac{\beta}{4}\right)T_{10} + \left(1 - \frac{\beta}{2}\right)T_{11} + \left(\frac{\beta}{4}\right)T_{12} \\
T_{12}' &= \left(\frac{\beta}{2}\right)T_{11} + \left(1 - \frac{\beta}{2}\right)T_{12}
\end{aligned}\right\} \quad (B1)$$

where

$$\gamma = \frac{q\ \Delta t}{cw\tau}$$

and

$$\beta = \frac{k\ \Delta t}{cw\tau^2}$$

All constants and coefficients in the above equations are known, except the magnitude of the time interval Δt which is determined by a convergence criterion outlined in references 7 and 9. The values of the coefficients of the above 12 equations can now be computed.

To facilitate the stepwise computation, the equations can be put in matrix form which includes the evaluated coefficients for routine mechanical computation.

The inclusion of the interface conductance can be accomplished by two distinct means as follows:

(1) The first method treats the interface as a simple series resistance between the two elements upstream and downstream of the interface. Thus, the heat transferred between lumps A and B, y distance apart and across an interface of conductance h, will be $\frac{\text{Area}(T_B - T_A)}{(y/k) + (l/h)}$ instead of $\frac{\text{Area} \times k(T_B - T_A)}{y}$. That is, the original resistance y/k between two neighboring lumps is increased by an amount l/h when the interface is interposed.

Accordingly, compared with the integral heat path, the heat-balance equations for the six lumps adjacent to the interface have to be modified in the following manner:

$$\left.\begin{aligned}
T_4' &= \gamma + \left(\tfrac{2}{3}\beta\right)T_3 + \left(1 - \tfrac{5}{3}\beta - \epsilon\right)T_4 + (\beta)T_5 + (\epsilon)T_7 \\
T_5' &= \gamma + (\beta)T_4 + (1 - 2\beta - \epsilon)T_5 + (\beta)T_6 + (\epsilon)T_8 \\
T_6' &= \gamma + (2\beta)T_5 + (1 - 2\beta - \epsilon)T_6 + (\epsilon)T_9 \\
T_7' &= (\epsilon)T_4 + (1 - \beta - \epsilon)T_7 + (\beta)T_8 \\
T_8' &= (\epsilon)T_5 + (\beta)T_7 + (1 - 2\beta - \epsilon)T_8 + (\beta)T_9 \\
T_9' &= (\epsilon)T_6 + (2\beta)T_8 + \left(1 - \tfrac{8}{3}\beta - \epsilon\right)T_9 + \left(\tfrac{2}{3}\beta\right)T_{10}
\end{aligned}\right\} \quad (B2)$$

where

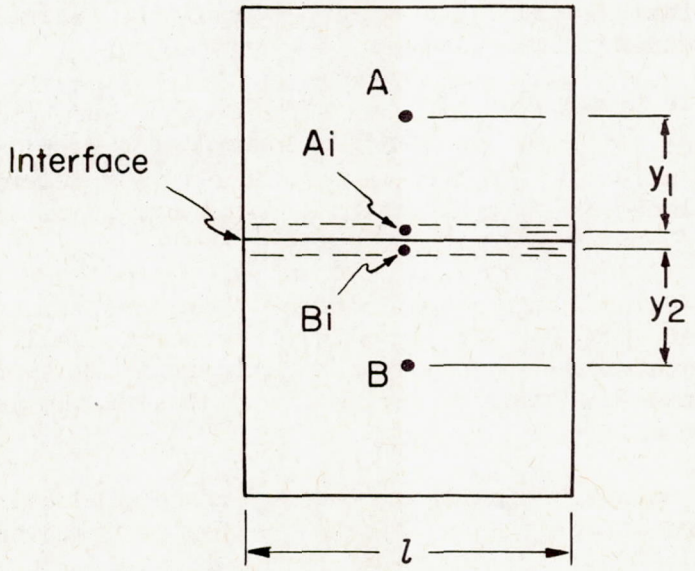
$$\epsilon = \frac{\Delta t}{cw\left(\frac{\tau^2}{k} + \frac{\tau}{h}\right)}$$

The expressions for the other lumps (eqs. (7)) do not change.

It can be seen that in the above method the only change in calculations due to the interface is a modification of some of the matrix coefficients. This, however, may also necessitate a change in the maximum allowable time interval Δt by the convergence criterion.

(2) An alternate, more exact method of including contact conductance has been developed (ref. 9) which does not impose a linear relationship on the instantaneous heat flow through the interface and the two half lumps on either side of it.

The method considers two elements of infinitesimal thickness next to the interface plane as shown in the following sketch:



These elements Ai and Bi approach zero volume in the limit; therefore, they can be assumed to transmit but not to store heat. Thus, the heat-balance equation for element Ai is

$$\frac{k}{y_1}\left(T_A - T_{Ai}\right) + h\left(T_{Bi} - T_{Ai}\right) = 0 \qquad \text{(B3a)}$$

and, for element Bi,

$$\frac{k}{y_2}\left(T_B - T_{Bi}\right) + h\left(T_{Ai} - T_{Bi}\right) = 0 \qquad (B3b)$$

Solving the equations simultaneously for T_{Ai} and T_{Bi} gives

$$T_{Ai} = \frac{T_A\left(k + hy_2\right) + T_B\left(hy_1\right)}{k + h\left(y_1 + y_2\right)} \qquad (B4a)$$

and

$$T_{Bi} = \frac{T_B\left(k + hy_1\right) + T_A\left(hy_2\right)}{k + h\left(y_1 + y_2\right)} \qquad (B4b)$$

It can be seen that, in this method, the interface limiting temperatures are prescribed functions of the adjacent large lump temperatures and different constants including physical dimensions, thermal conductivity, and interface conductance value.

Not only is the computation of temperatures T_{Ai} and T_{Bi} at the end of each time interval necessary to arrive at the net ΔT across the interface, but also the interface temperatures thus determined are used in the heat balance of some of the original large lumps in the next interval.

In the so-called "marching process," therefore, an additional step is involved. After each step in the matrix computation all interface temperatures are computed from simultaneous equations of the type of equations (B4a) and (B4b) and then inserted at the proper places in the matrix of the next interval and so on.

The first method of including the interface conductance value is evidently a more direct one but has the following disadvantages:

(a) It does not yield temperatures immediately at the interface; therefore, ΔT is not accurately known.

(b) The transient heat flow during any time interval Δt necessarily turns out to be the same across the interface as it is in both half lumps straddling the interface plane. However, it is obvious that the transient temperature gradient, and thus the rate of heat storage, at any instant should be higher at locations upstream and lower at locations downstream of the interface as pointed out in the section entitled "Discussion."

The second method remedies both of the above disadvantages simultaneously and is therefore considered superior to the first one, but the calculation procedure becomes more laborious.

The temperature functions found by any of the above methods are considered continuous since the time interval which assures convergence is usually very small, a fraction of a second in most practical cases. High-speed digital computers are ideally suited to carry out the mechanically simple but tedious calculations. In the typical 12-lump subdivision shown above, 38 multiplications and 12 additions were involved in each small interval and 6 steps were necessary to cover 1 second.

Numerical calculations were carried out for one specimen configuration duplicating as closely as possible the boundary conditions imposed in the corresponding experiments. Transient temperature distributions for short heating cycles were calculated for both the continuous heat path of the integral specimen and the discontinuous fabricated version. For the fabricated specimen both of the above methods of including interface conductance were utilized.

The numerical solutions and experimental results showed a satisfactory but not exact correspondence. The slight discrepancy between the two may be attributed to

(a) Failure to duplicate the experimental boundary conditions exactly in the calculations

(b) Uncertainty in the thermal conductivity and diffusivity of the specimen material, as explained in the section "Precision of Data"

(c) Uncertainty in and transient variability of the interface conductance value, as explained in the section "Discussion"

REFERENCES

1. Barzelay, Martin E., Tong, Kin Nee, and Hollo, George: Thermal Conductance of Contacts in Aircraft Joints. NACA TN 3167, 1954.

2. Barzelay, Martin E., Tong, Kin Nee, and Holloway, George F.: Effect of Pressure on Thermal Conductance of Contact Joints. NACA TN 3295, 1955.

3. Coulbert, C. D., and Liu, C.: Thermal Resistance of Aircraft Structure Joints. Tech. Note 53-50, Contract AF-33(616)-293, WADC and Dept. Eng., Univ. of Calif., June 1953.

4. Baker, H. D., Ryder, E. A., and Baker, N. H.: Temperature Measurement in Engineering. Vol. 1. John Wiley & Sons, Inc., 1953.

5. Evans, J. E., Jr.: Thermal Conductivity of 14 Metals and Alloys Up to 1100° F. NACA RM E50L07, 1951.

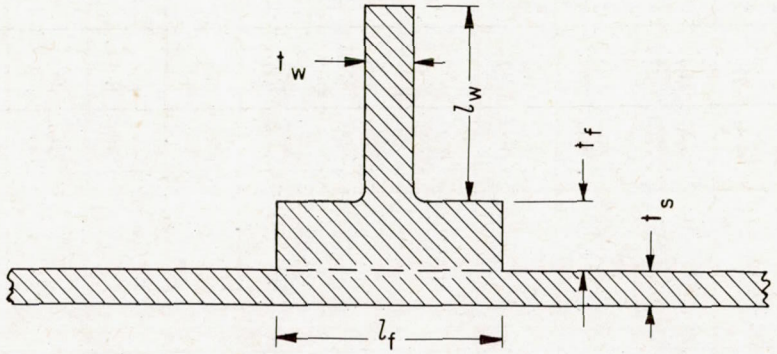
6. Jakob, Max: Heat Transfer. Vol. I. John Wiley & Sons, Inc., c.1949.

7. Dusinberre, G. M.: Numerical Analysis of Heat Flow. First Ed., McGraw-Hill Book Co. Inc., 1949.

8. Quinville, J. A., and Gordon, C. K.: Transient Temperature Distribution in Typical Aircraft Structures Due to Aerodynamic Heating - Lumped Parameter Solution. Rep. No. NAI-54-454, Northrop Aircraft Inc., June 30, 1954.

9. Holloway, G. F.: The Effect of an Interface on the Transient Temperature Distribution in Composite Aircraft Joints. Thesis, Syracuse Univ., 1954.

TABLE I.- SPECIMEN DIMENSIONS



Specimen		Thickness of skin, t_s, in.	Length of flange, l_f, in.	Thickness of flange, t_f, in.	Length of web, l_w, in.	Thickness of web, t_w, in.	Rivet type in fabricated specimen
Fabricated	Integral (a)						
b_1	1C	0.125	0.500	0.375	0.500	0.125	AD-3
c_2	2C	.125	.500	.125	.500	.125	AD-2
b_3	3C	.125	.500	.042	.500	.125	AD-3
b_4	4C	.125	1.250	.125	1.250	.125	AD-4
c_5	5C	.125	1.000	.250	1.000	.250	AD-3
c_6	6C	.250	.500	.125	.500	.125	AD-2
b_7	7C	.125	.375	.125	1.250	.125	AD-2
b_8	8C	.125	.750	.250	2.500	.250	AD-3
c_9	9C	.125	.625	.125	.125	.125	AD-2
c_{10}	10C	.125	1.250	.250	.250	.250	AD-4
b_{11}	11C	.250	1.250	.125	1.250	.125	AD-4
b_{12}	12C	.250	.375	.125	1.250	.125	AD-2
c_{13}	13C	.250	.625	.125	.125	.125	AD-2
c_{14}	14C	.250	1.250	.250	1.250	.250	AD-4
b_{15}	15C	.064	1.250	.064	1.250	.064	AD-4

[a]Made in shop 3.

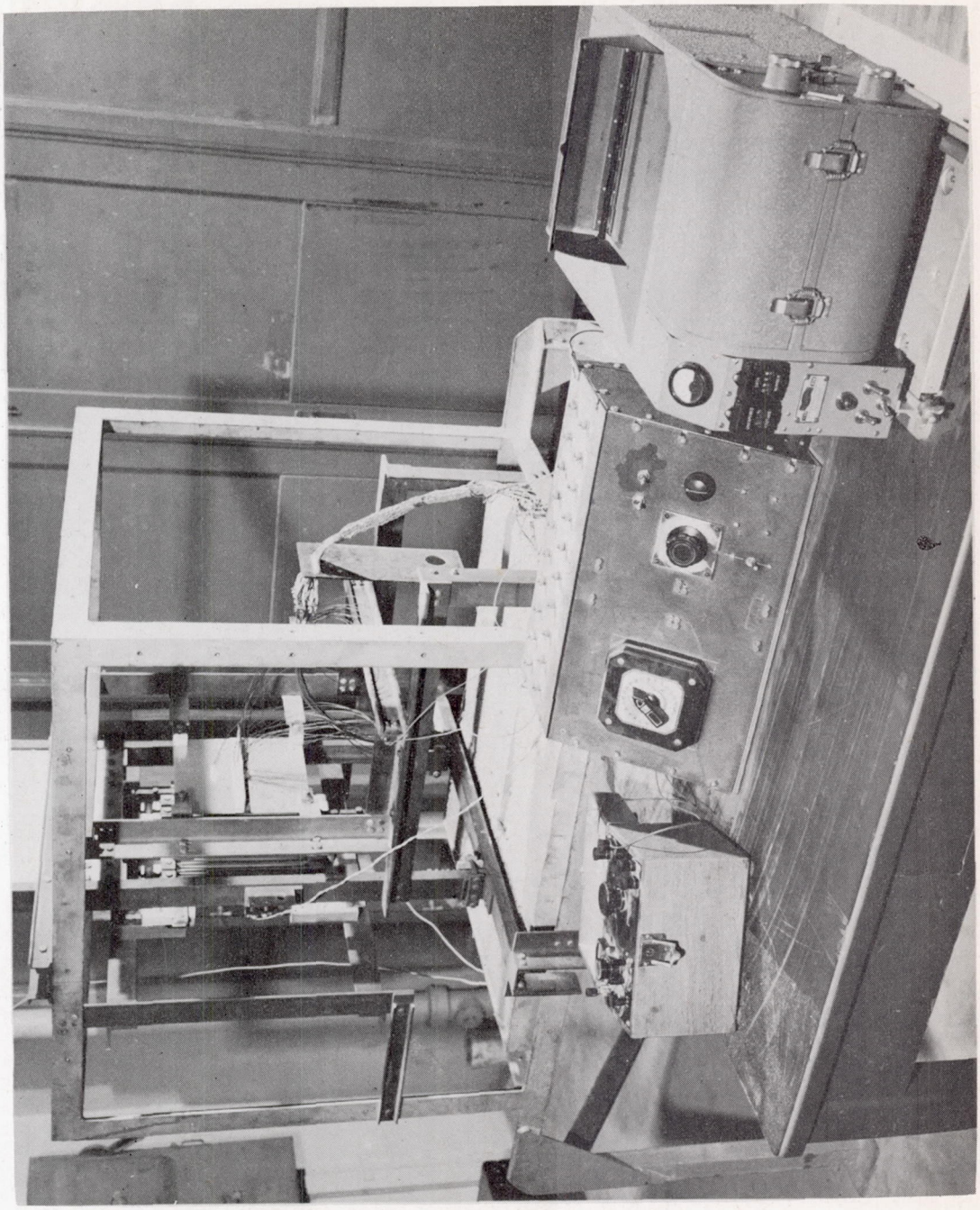
[b]Made in shop 1.

[c]Made in shop 2.

TABLE II.- EXPERIMENTAL INTERFACE CONDUCTANCE VALUES

Specimen	Test series 1				Test series 2			
	Heat input, Q, $\frac{\text{Btu}}{(\text{sq ft})(\text{sec})}$	Interface conductance, h, $\frac{\text{Btu}}{(\text{sq ft})(\text{hr})(^\circ\text{F})}$		Equivalent air-gap thickness, δ, in.. (a)	Heat input, Q, $\frac{\text{Btu}}{(\text{sq ft})(\text{sec})}$	Interface conductance, h, $\frac{\text{Btu}}{(\text{sq ft})(\text{hr})(^\circ\text{F})}$		Equivalent air-gap thickness, δ, in. (a)
1	7.44	Min. Max.	570 643	0.32×10^{-3} .28	31.6	Min. Max.	269 323	0.67×10^{-3} .56
2	12.4	Min. Max.	448 525	0.40 .34	20.3	Min. Max.	319 338	0.56 .53
3	4.40	Min. Max.	521 685	0.35 .26	27.8	Min. Max.	589 752	0.31 .24
4	5.27	Min. Max.	960 1,310	0.19 .14	23.3	Min. Max.	623 842	0.29 .21
5	12.1	Min. Max.	204 301	0.88 .60	26.0	Min. Max.	156 213	1.15 .85
6	30.5	Min. Max.	334 414	0.54 .43	9.58	Min. Max.	275 313	0.65 .58
7	7.10	Min. Max.	322 398	0.56 .45	26.4	Min. Max.	156 231	1.15 .78
8	6.65	Min. Max.	578 946	0.31 .19	32.9	Min. Max.	613 734	0.29 .25
9	12.3	Min. Max.	412 619	0.44 .29	29.4	Min. Max.	323 490	0.56 .37
10	6.73	Min. Max.	935 1,030	0.19 .17	25.0	Min. Max.	855 913	0.21 .20
11	7.09	Min. Max.	342 479	0.53 .38	33.5	Min. Max.	282 321	0.64 .56
12	10.7	Min. Max.	326 459	0.55 .39	37.8	Min. Max.	220 291	0.82 .62
13	7.29	Min. Max.	297 500	0.61 .36	36.0	Min. Max.	297 434	0.61 .41
14	7.44	Min. Max.	268 385	0.67 .47	30.3	Min. Max.	195 242	0.92 .74
15	4.92	Min. Max.	239 304	0.75 .59	23.3	Min. Max.	171 237	1.05 .76

[a]Equivalent air gap is based on value of air thermal conductivity at 75° F, 3.47×10^{-7} Btu/(in.)(sec)(°F).



L-95756

Figure 1.- Overall view of test installation.

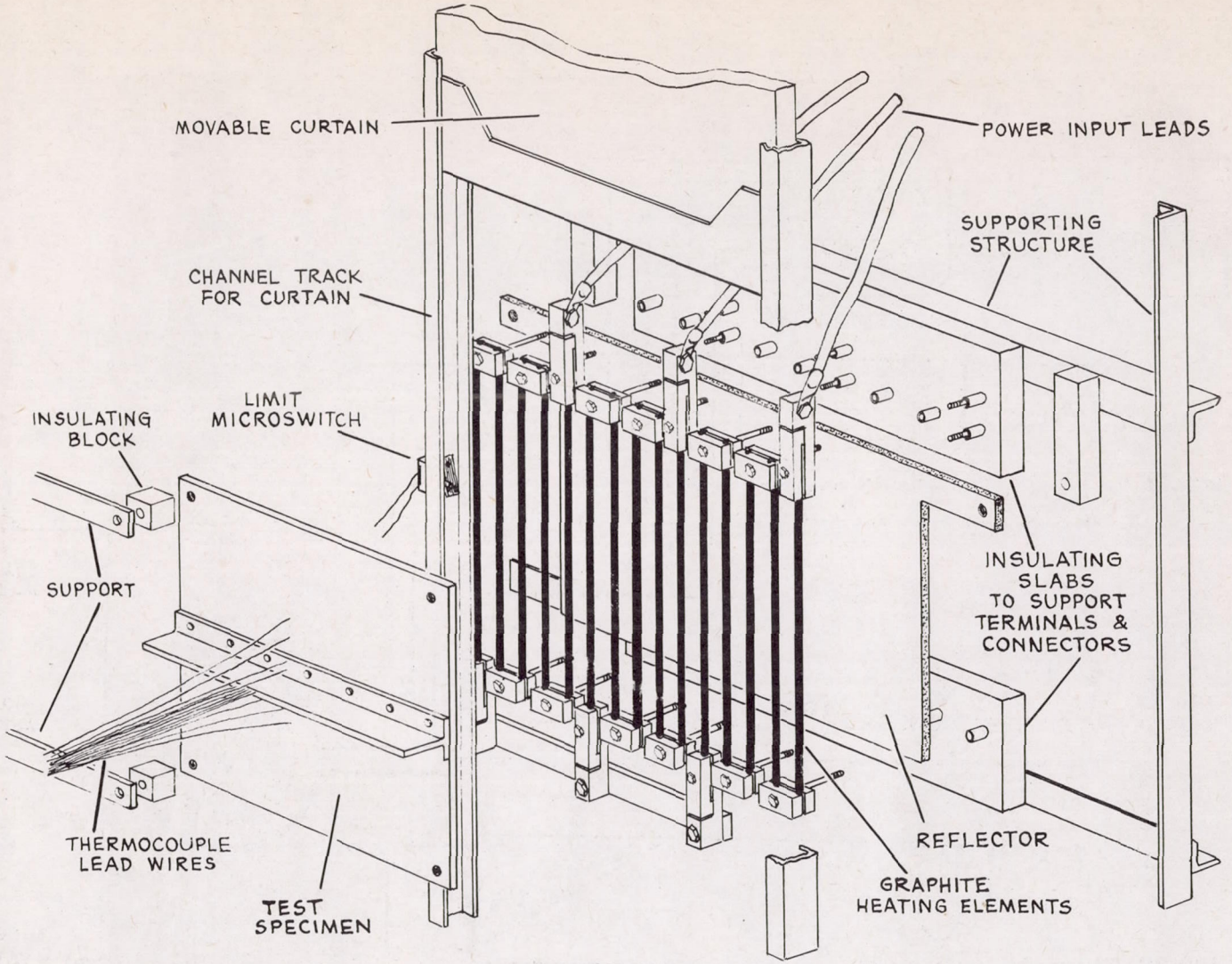


Figure 2.- Detailed exploded view of apparatus.

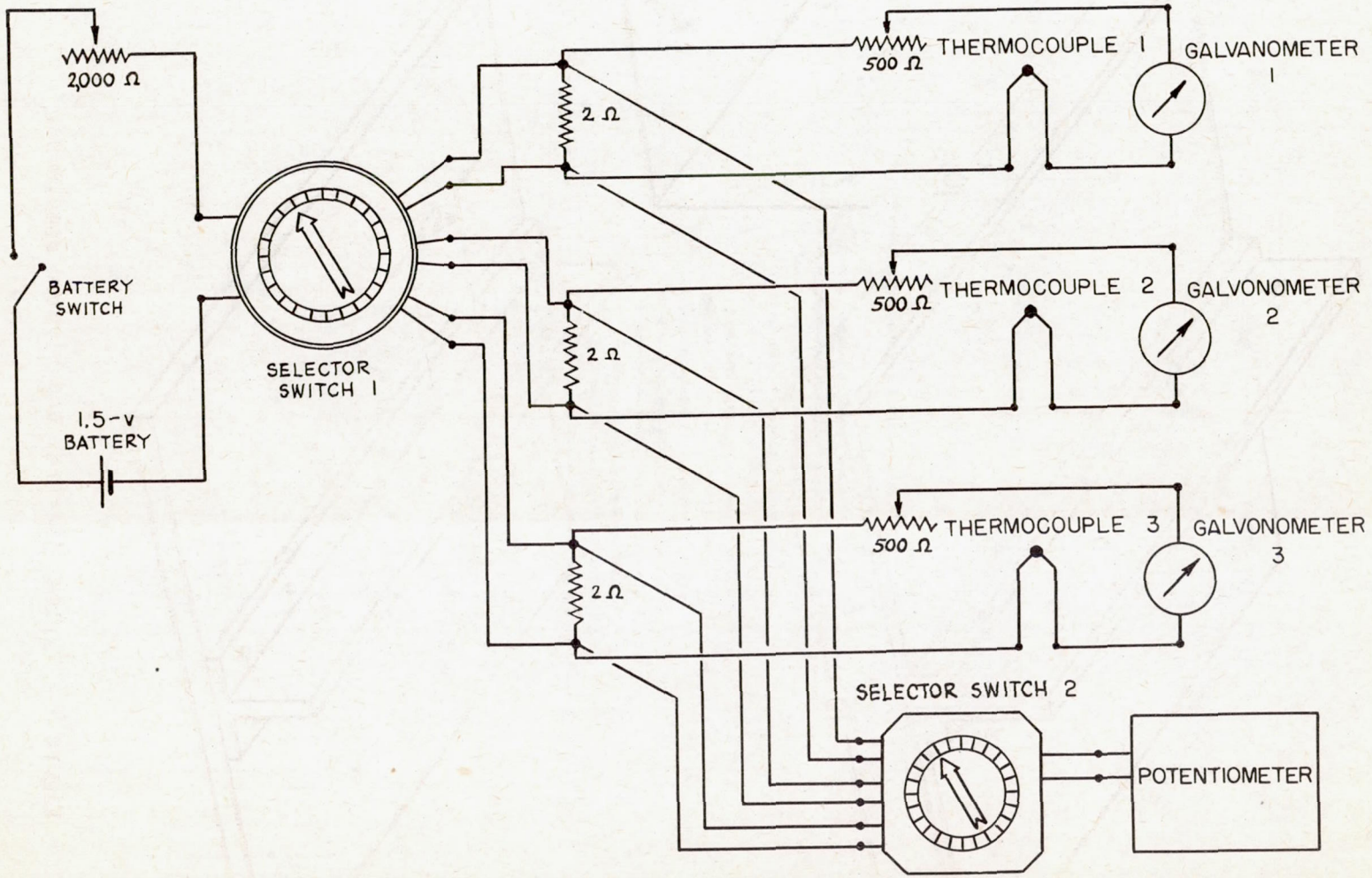


Figure 3.- Galvanometer and thermocouple calibrating circuits (three channels shown).

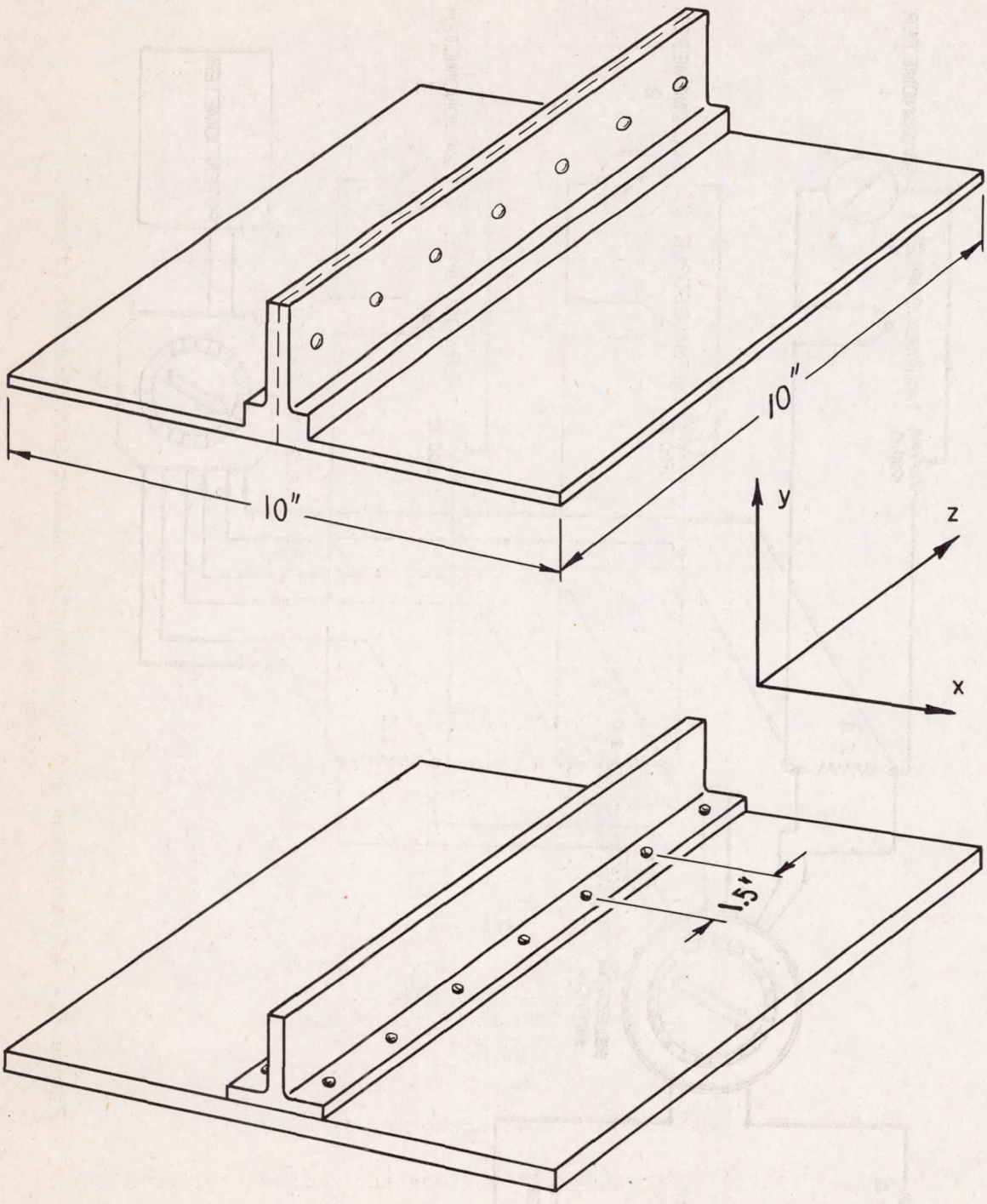
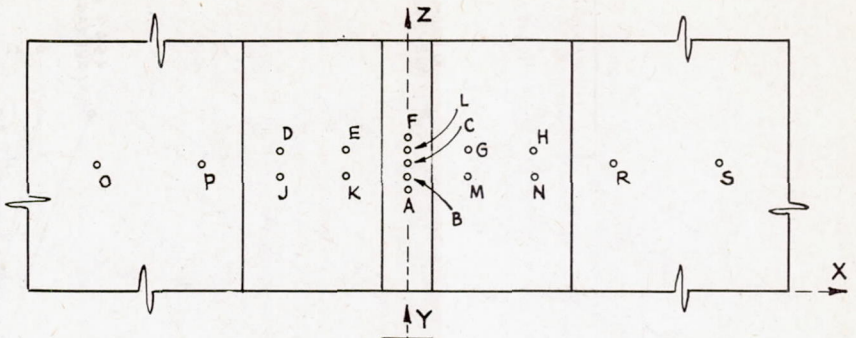
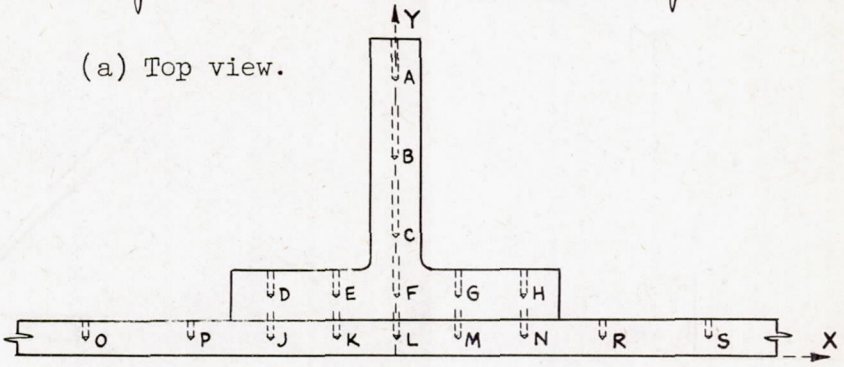


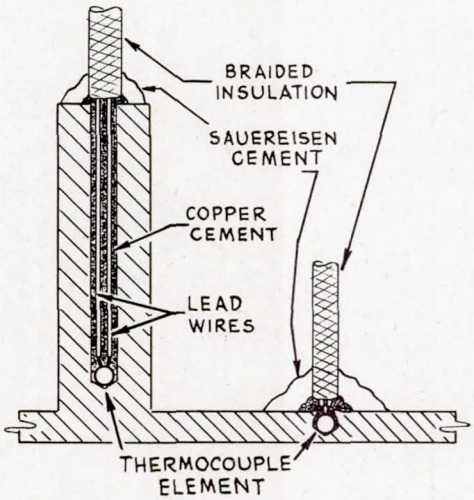
Figure 4.- Typical integral and riveted specimens.



(a) Top view.

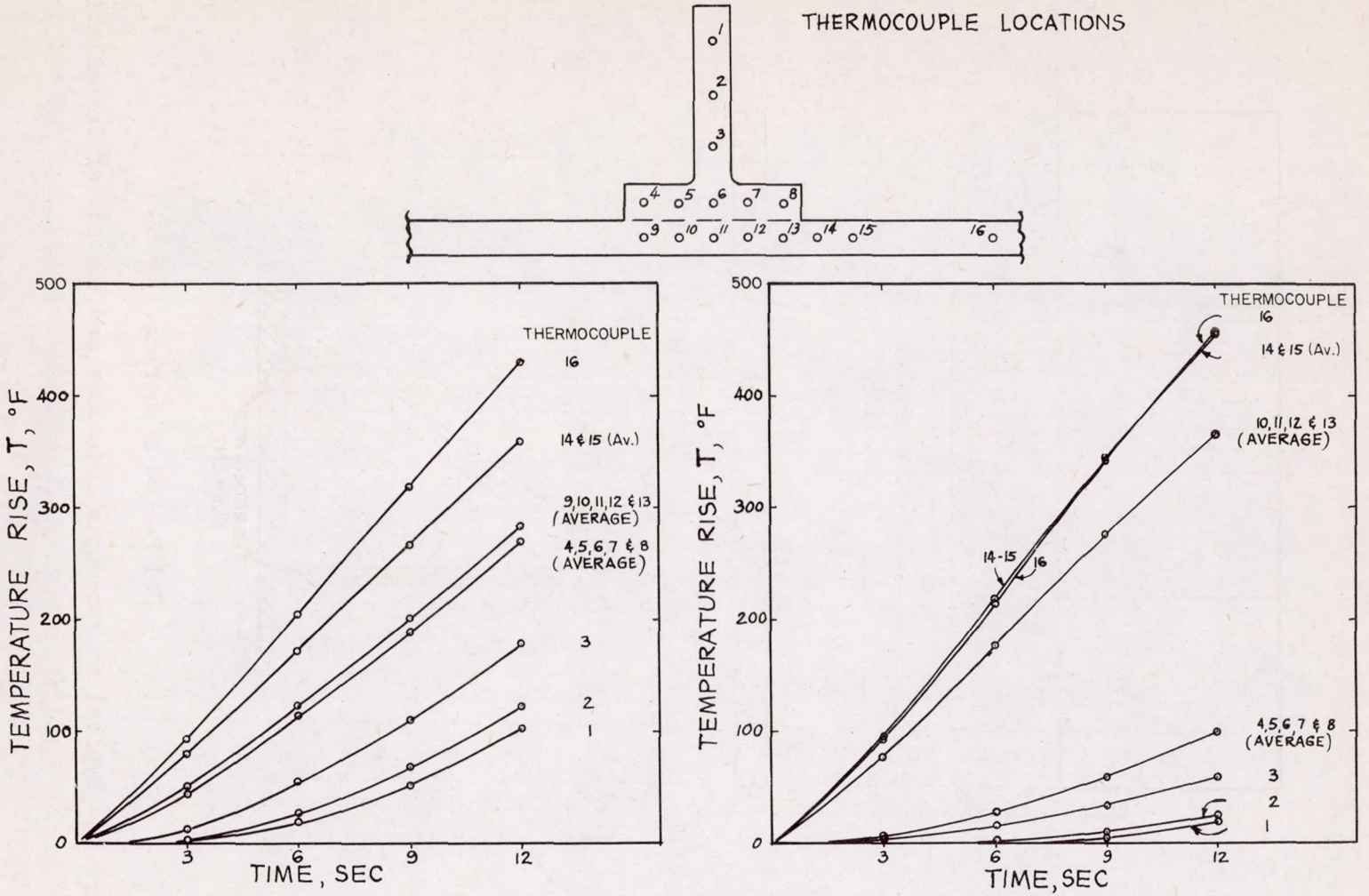


(b) End view.



(c) Peened anchoring.

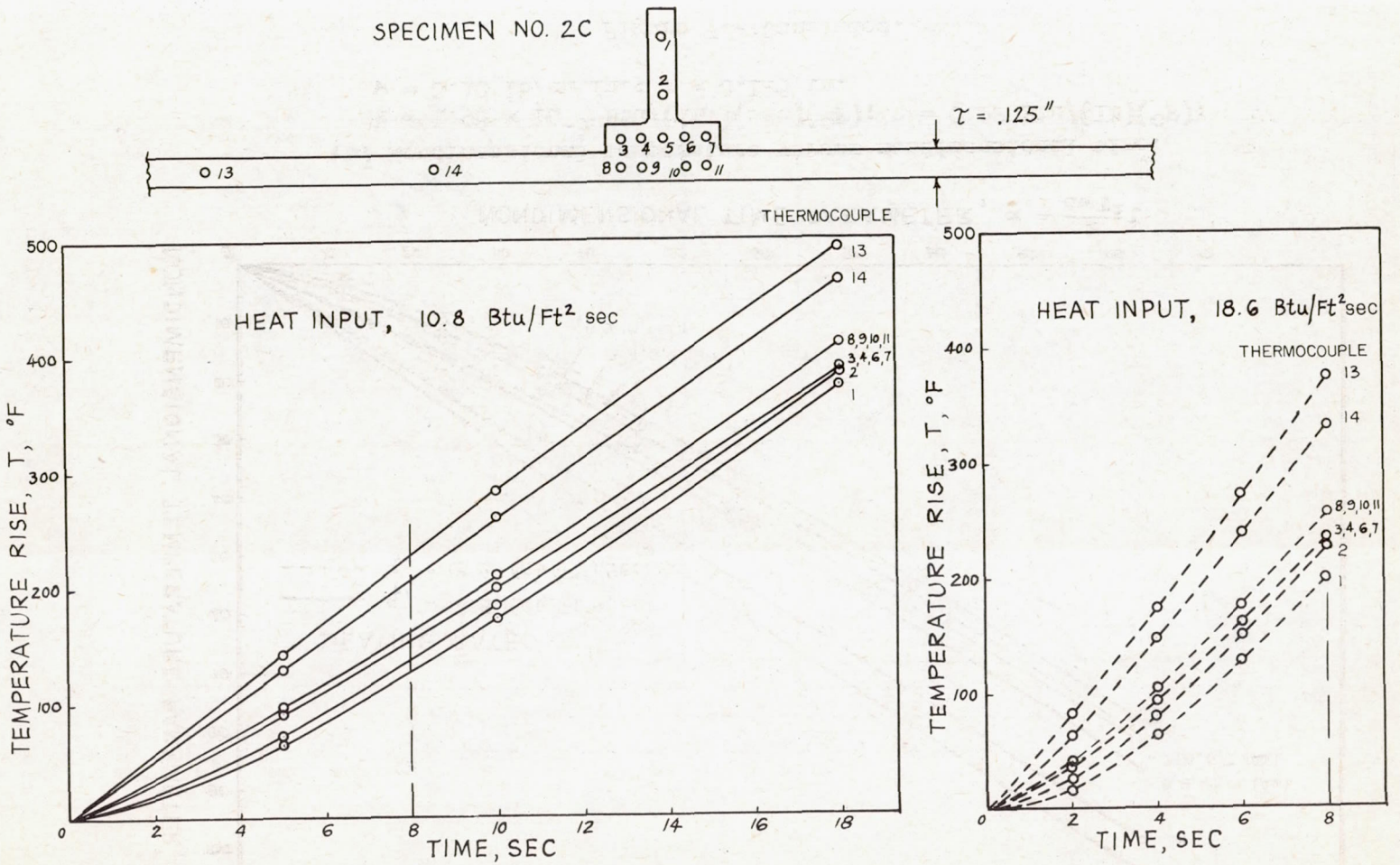
Figure 5.- Typical thermocouple locations and methods of installation.



(a) Integral specimen 14C.

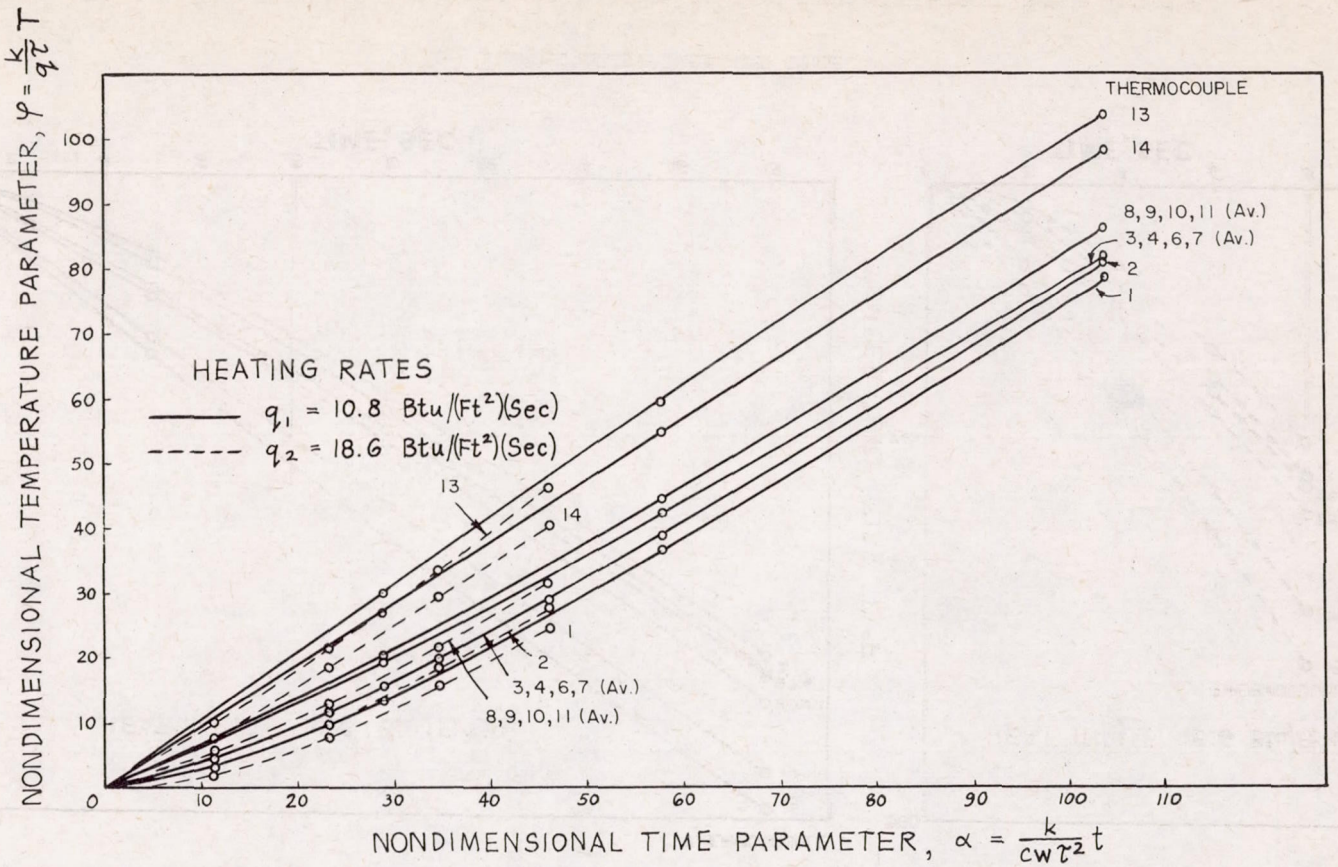
(b) Fabricated specimen 14.

Figure 6.- Typical temperature histories.



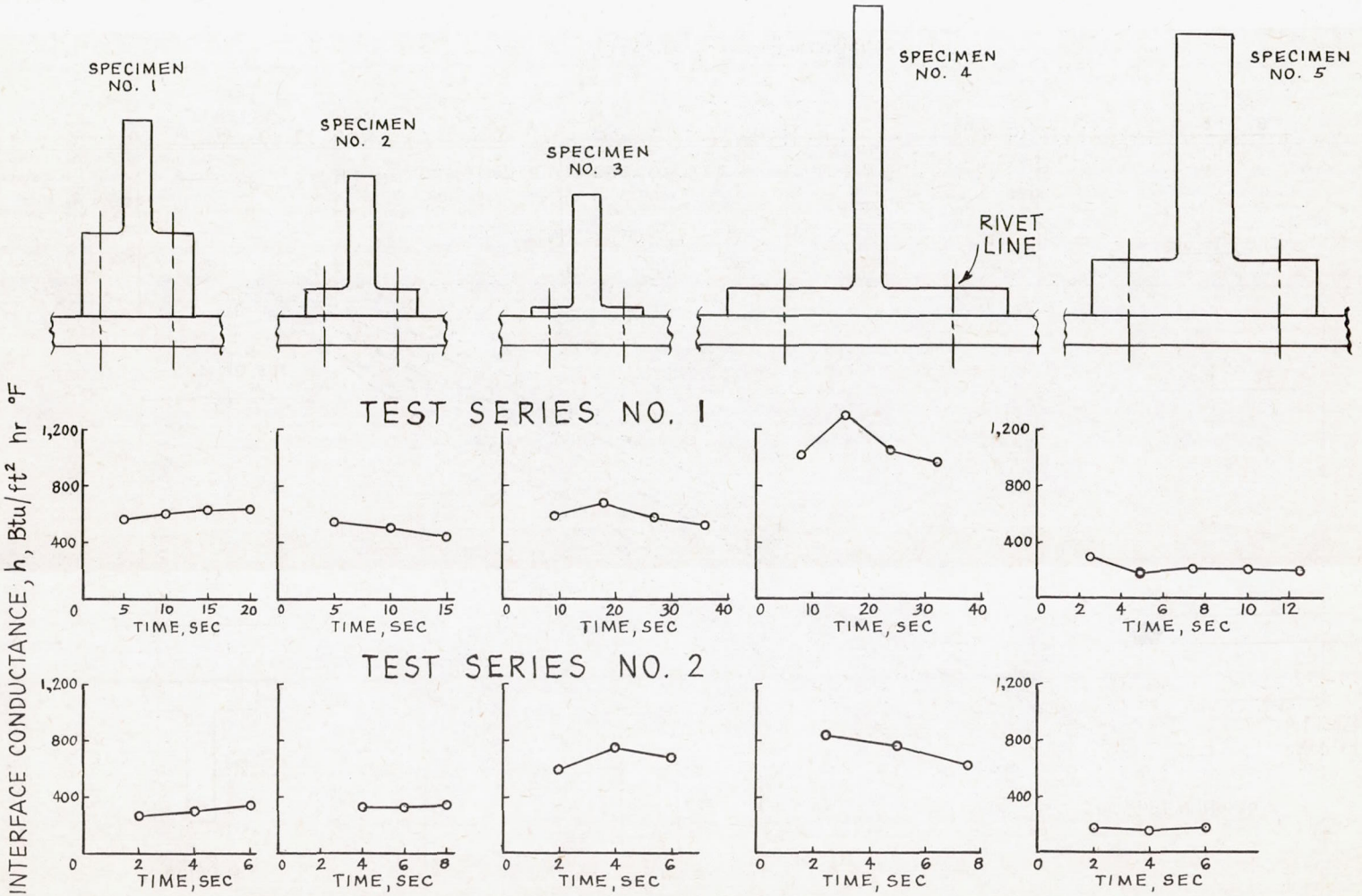
(a) Temperature versus time.

Figure 7.- Typical temperature histories for two different heat inputs (specimen 2C).



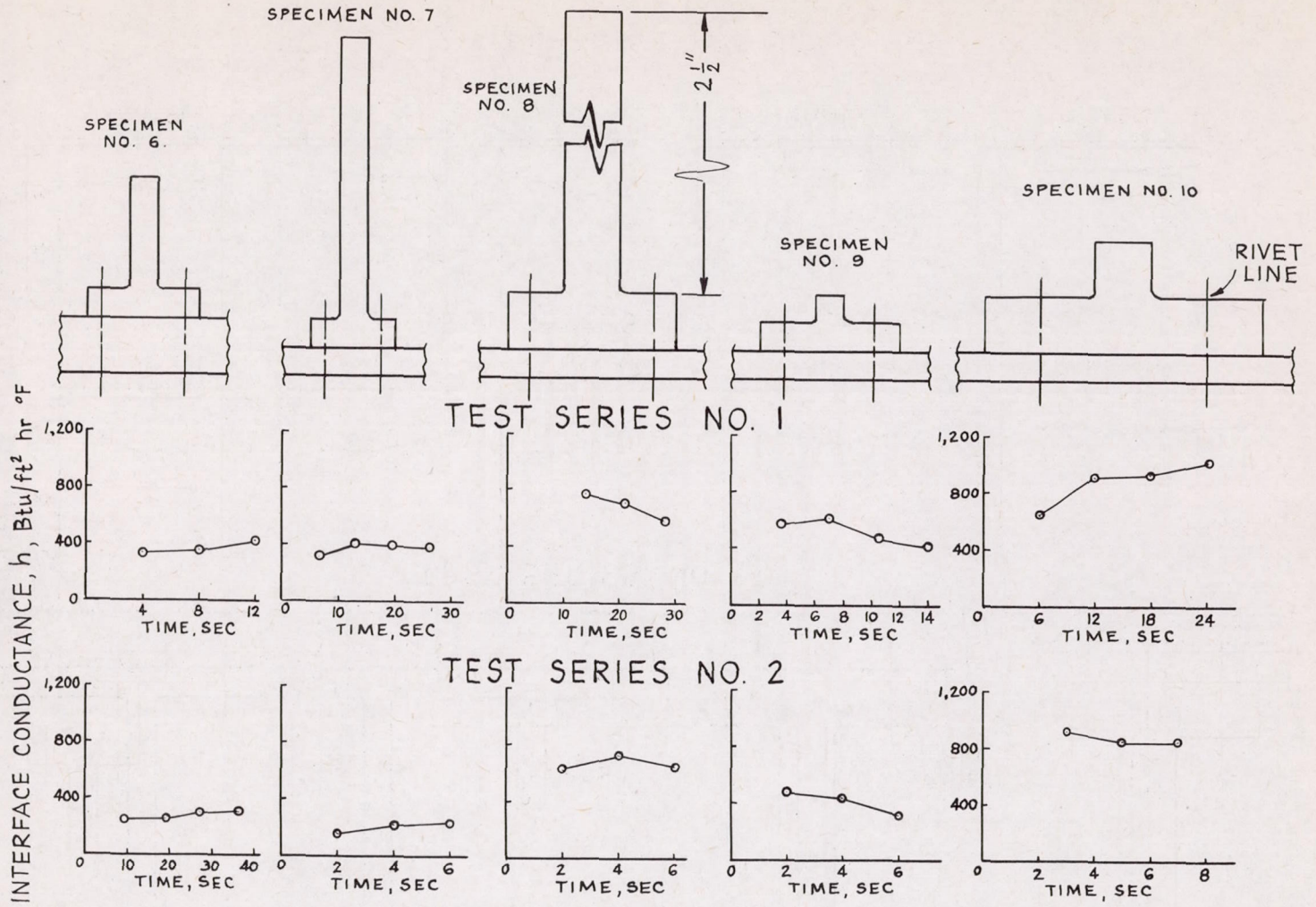
(b) Nondimensional temperature versus nondimensional time. $k = 1.98 \times 10^{-3}$ Btu/(in.)(sec)(°F); c = 0.22 Btu/(lb)(°F); w = 0.10 lb/cu in.; τ = 0.125 in.

Figure 7.- Concluded.



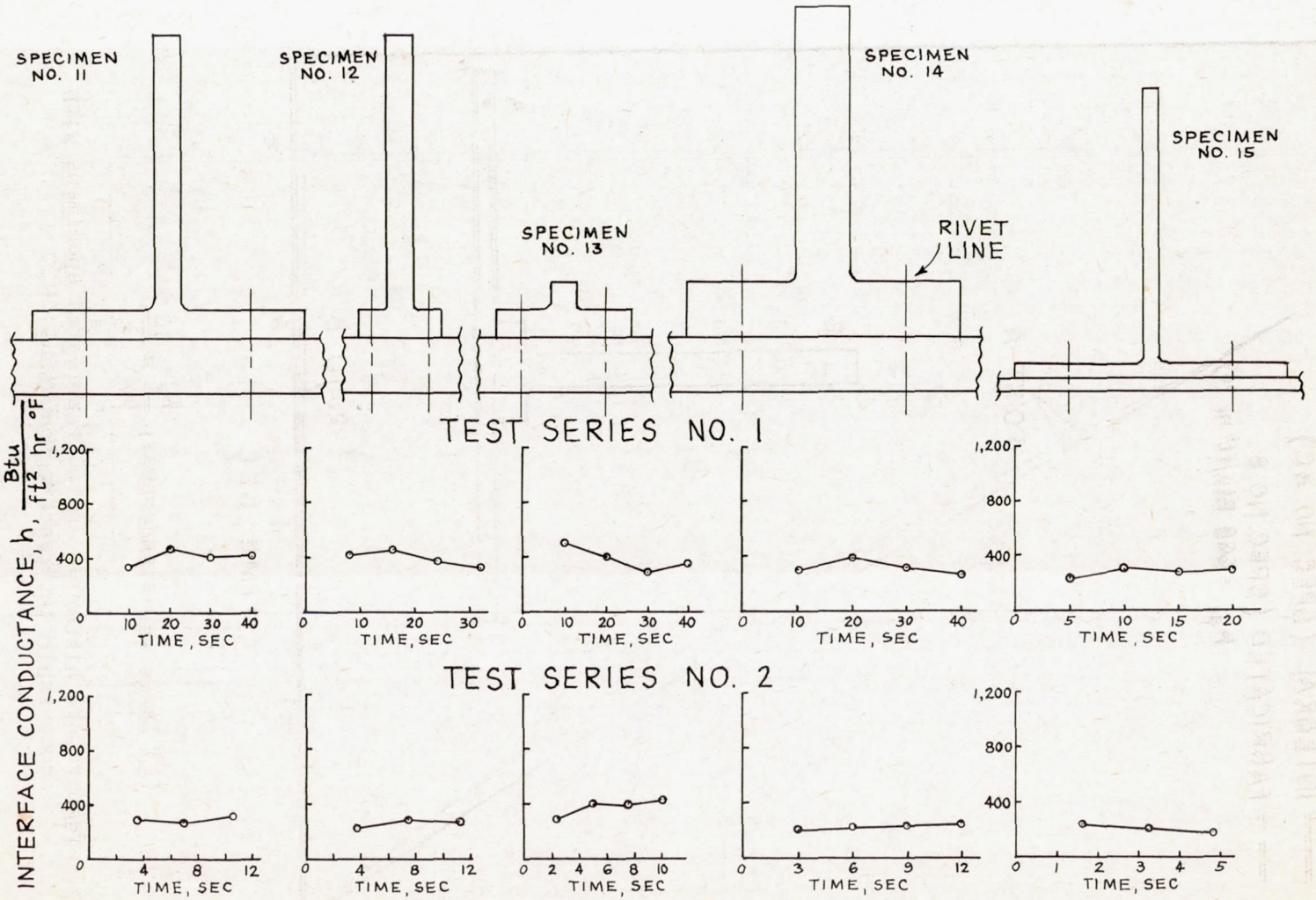
(a) Specimens 1 to 5.

Figure 8.- Experimental values of interface conductance.



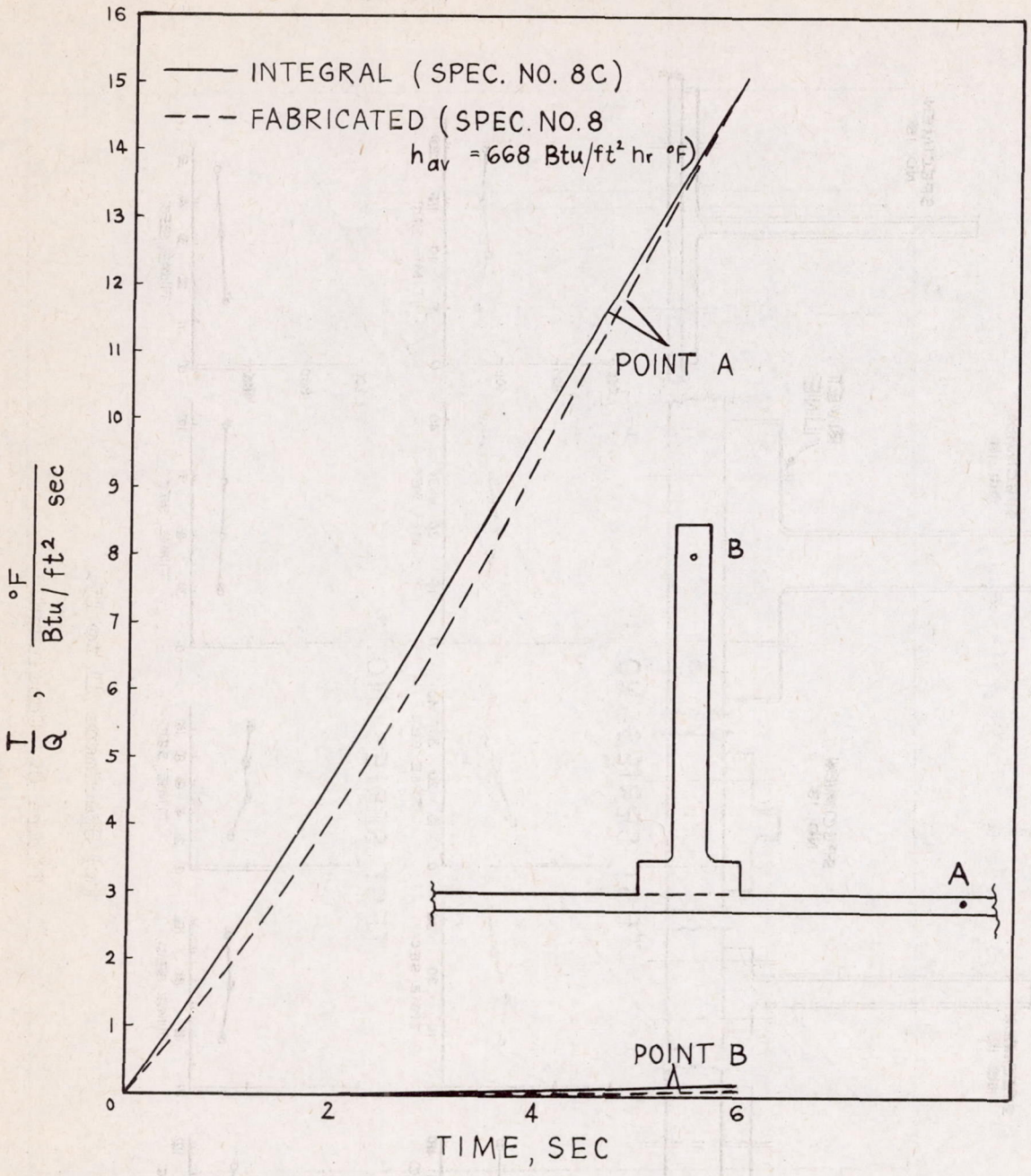
(b) Specimens 6 to 10.

Figure 8.- Continued.



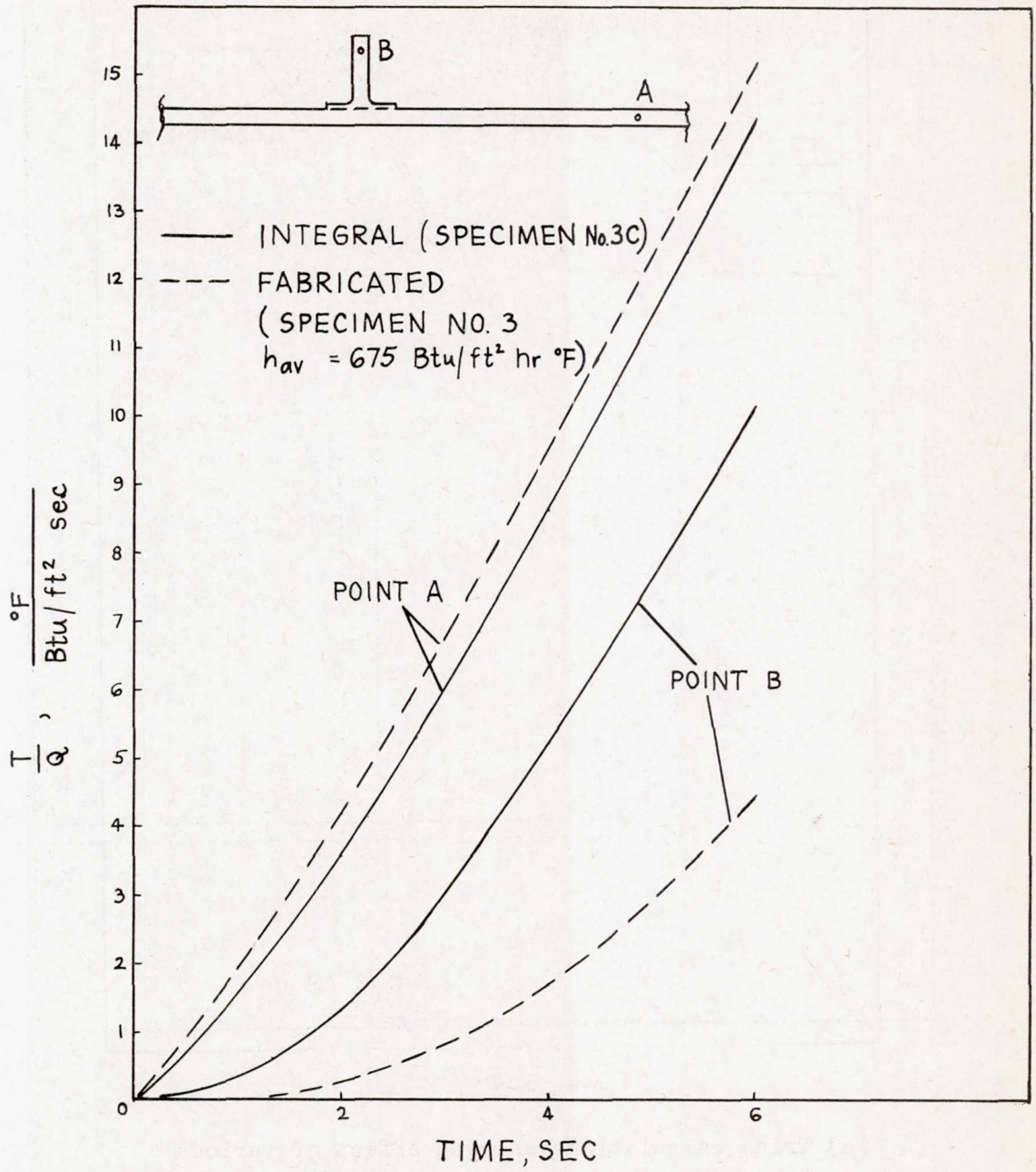
(c) Specimens 11 to 15.

Figure 8.- Concluded.



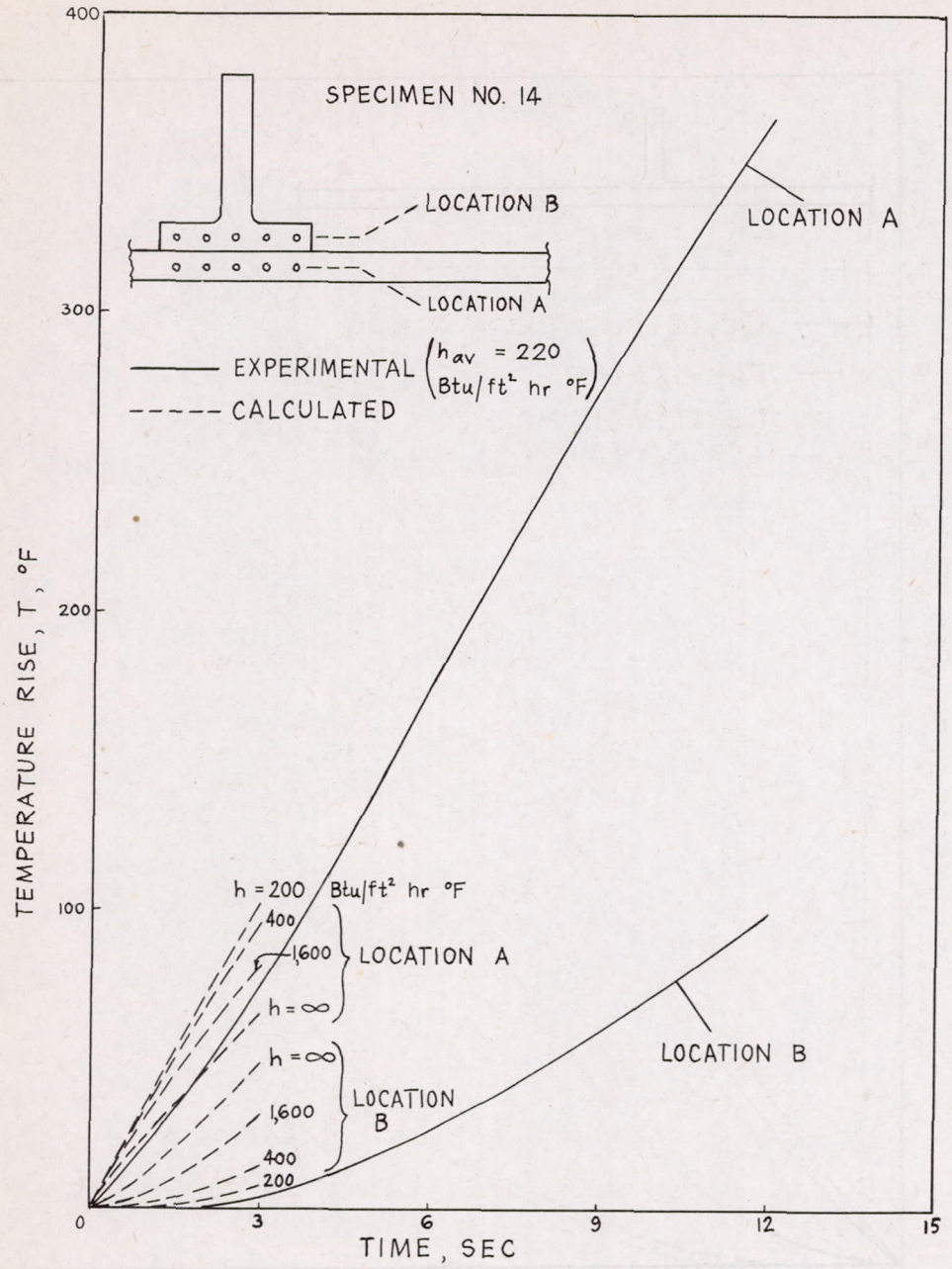
(a) Large web slenderness; $\frac{l_w}{t_w} = \frac{10}{1}$.

Figure 9.- Temperature histories in two fabricated specimens with comparable interface conductance.



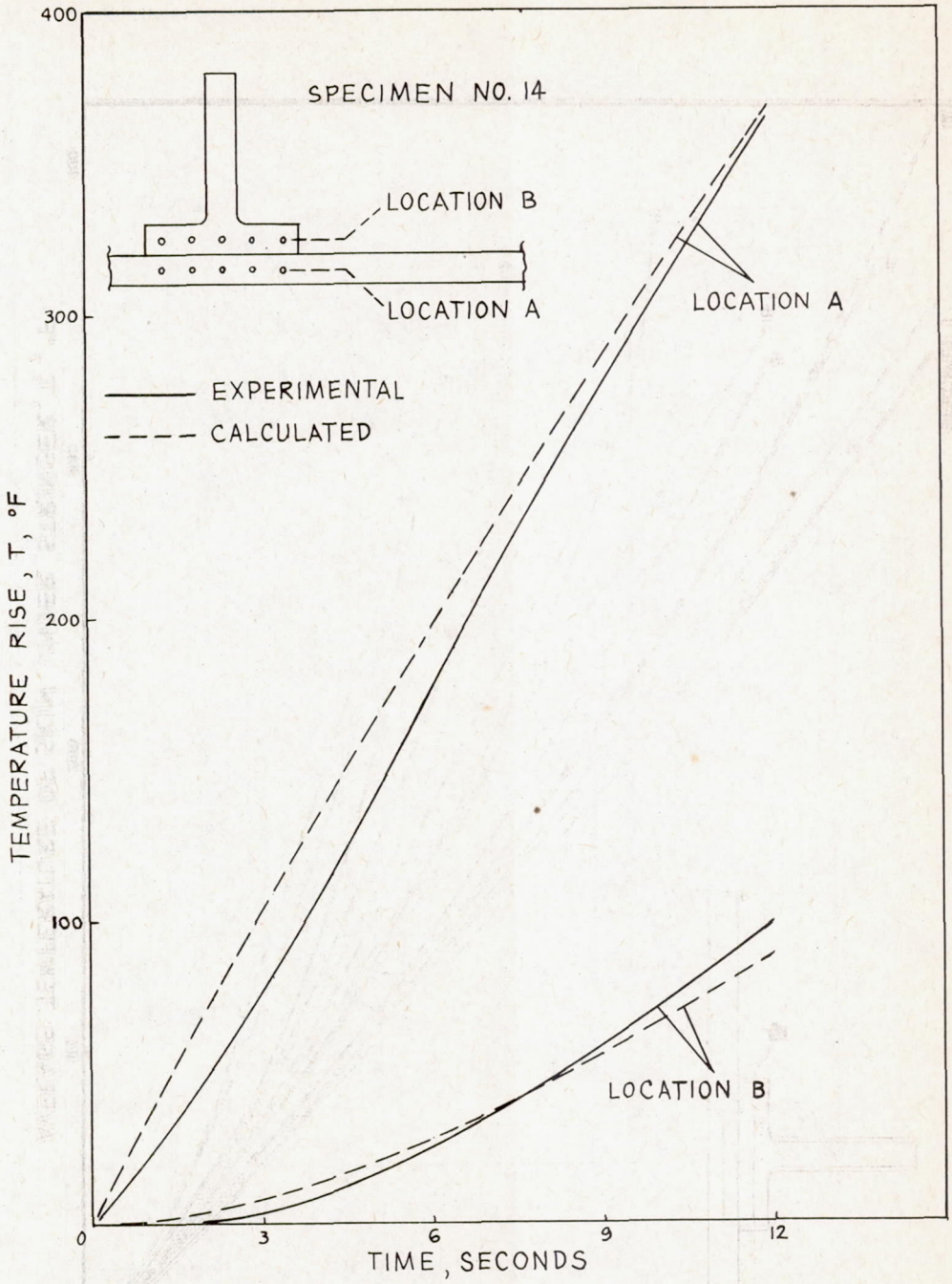
(b) Intermediate web slenderness; $\frac{l_w}{t_w} = \frac{4}{1}$.

Figure 9.- Concluded.



(a) Trial calculations showing effect of various interface conductance values.

Figure 10.- Comparison of experimental and calculated transient temperature distributions. Experimental curves are plotted for average of five points at each location.



(b) Final calculation with interface conductance of 200 Btu/(sq ft)(hr)(°F). All curves are plotted for average of five points at each location.

Figure 10.- Concluded.

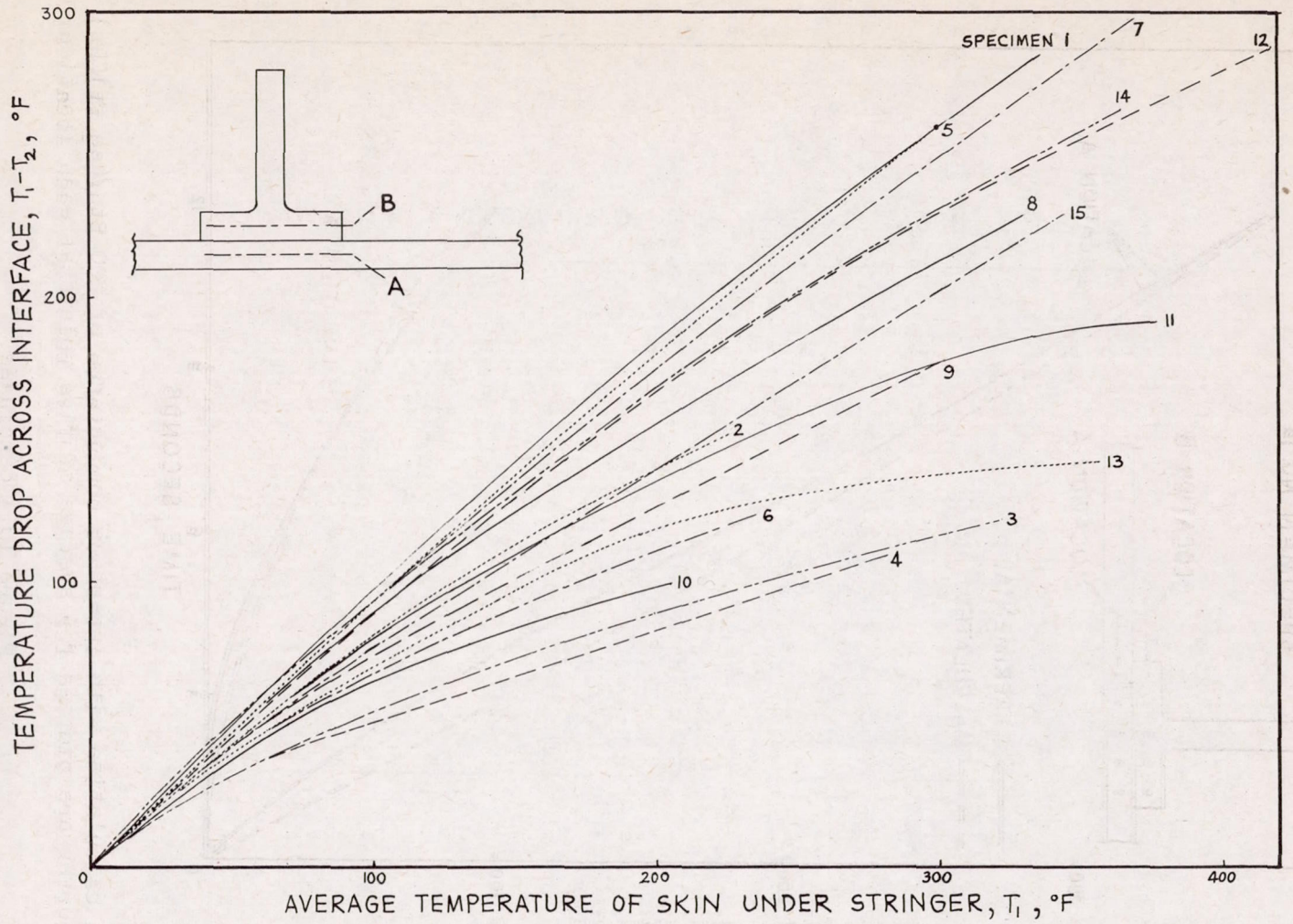
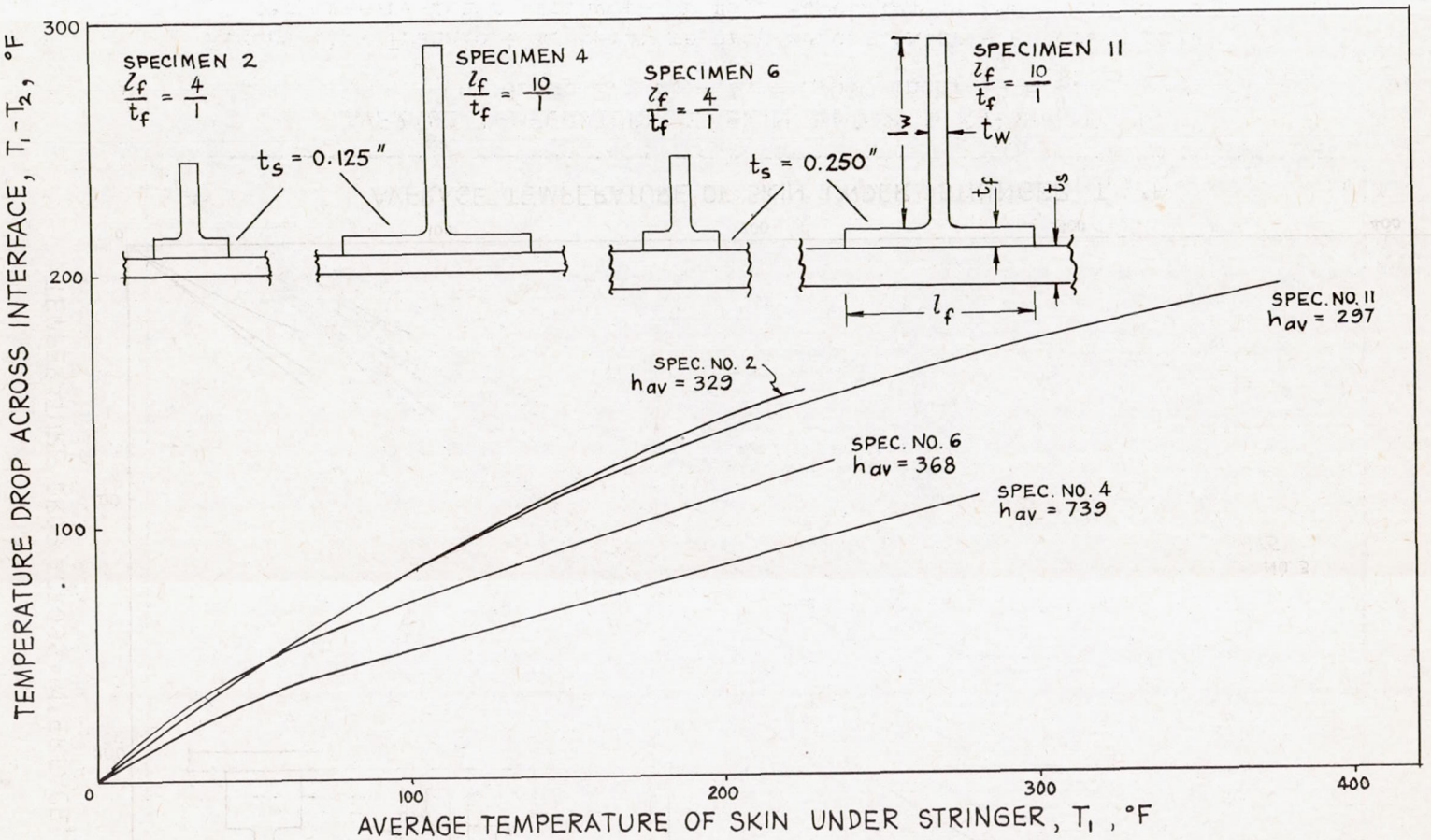
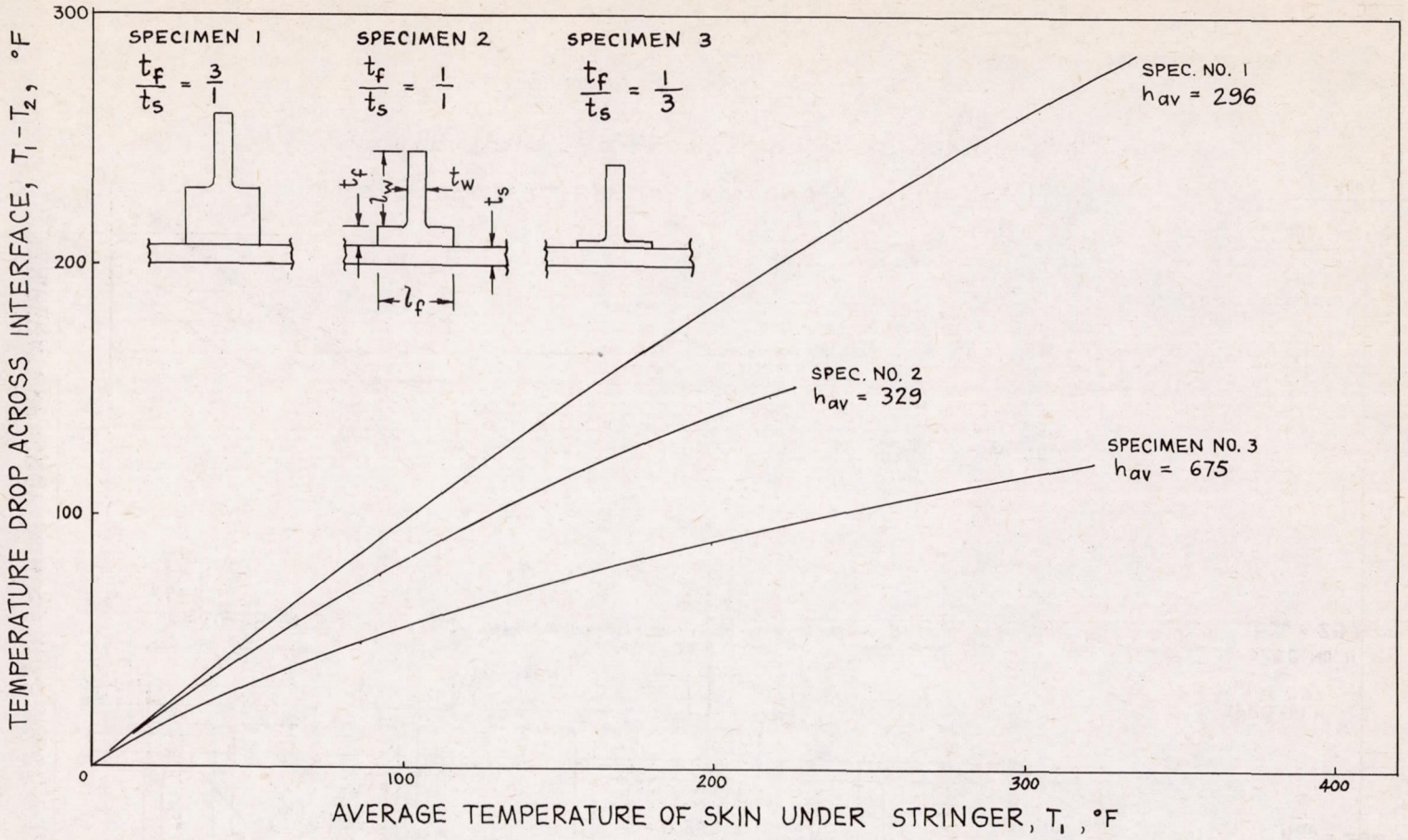


Figure 11.- Transient temperature drop across interface versus skin temperature under stringer for all geometries tested. T_1, average temperature at station A; T_2, average temperature at station B.



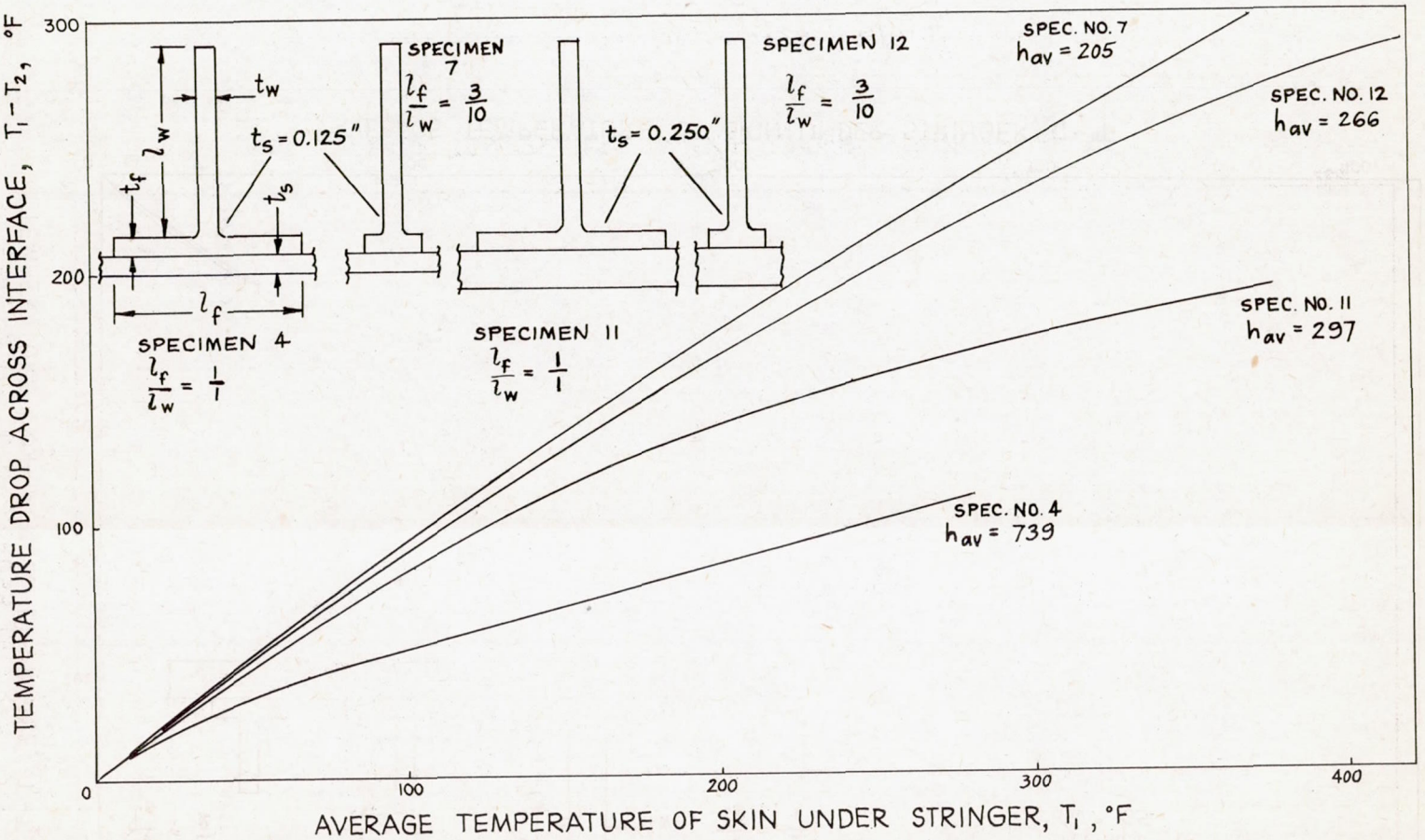
(a) Group 1. $t_f = t_w = 0.125$ inch; $\frac{l_f}{l_w} = \frac{1}{1}$.

Figure 12.- Effect of geometry on interface temperature-drop history.



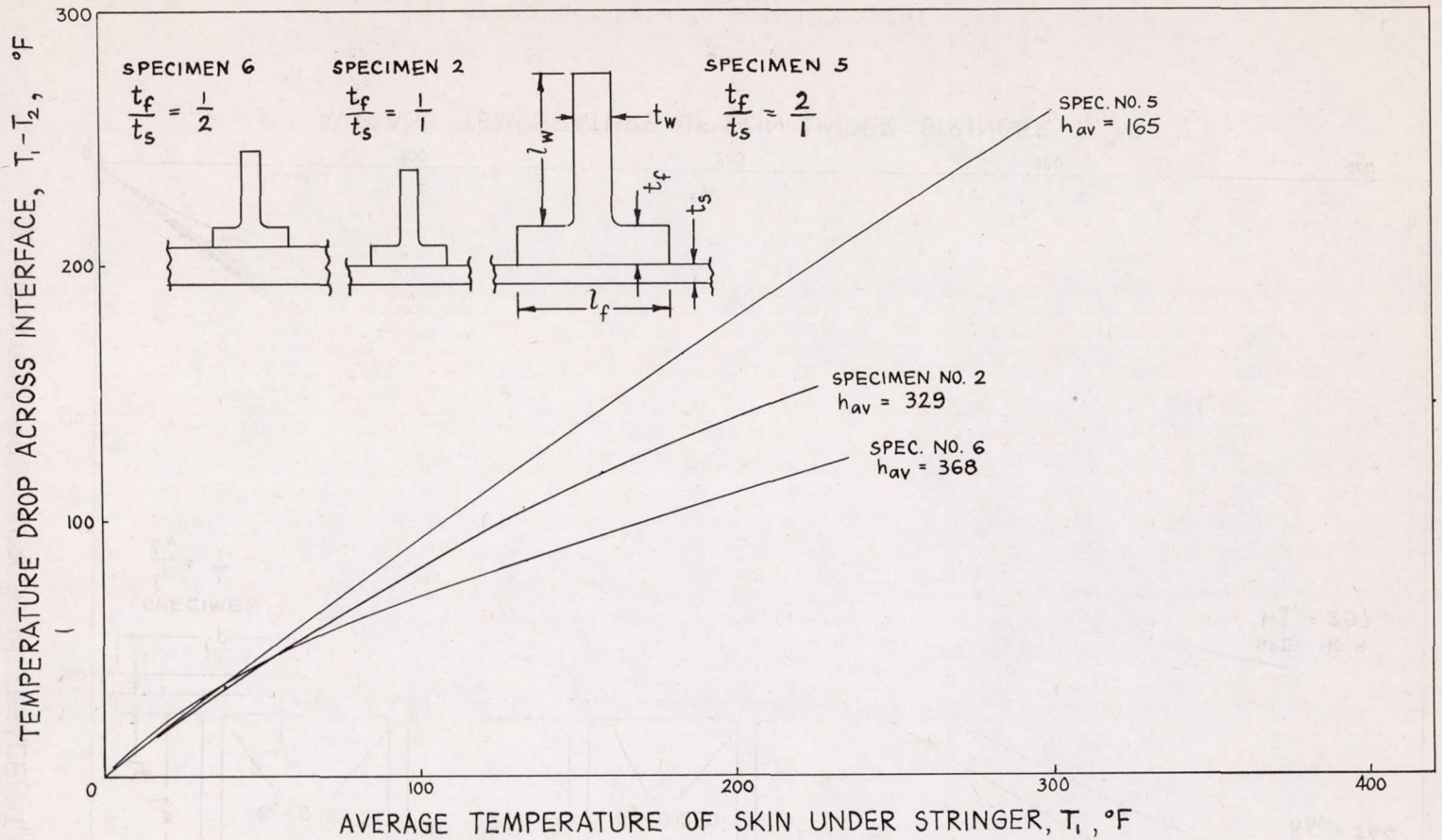
(b) Group 2. $l_f = l_w = 0.500$ inch; $\frac{l_w}{t_w} = \frac{4}{1}$.

Figure 12.- Continued.



(c) Group 3. $t_f = t_w = 0.125$ inch; $\frac{l_w}{t_w} = \frac{10}{1}$.

Figure 12.- Continued.



(d) Group 4. $\frac{l_f}{l_w} = \frac{1}{1}$; $\frac{l_f}{t_f} = \frac{l_w}{t_w} = \frac{4}{1}$.

Figure 12.- Concluded.

NACA - Langley Field, Va.